Boron Isotopes in Foraminifera: Systematics, Biomineralisation, and CO_2 Reconstruction

5

James W.B. Rae

Abstract

The boron isotope composition of foraminifera provides a powerful tracer for CO_2 change over geological time. This proxy is based on the equilibrium of boron and its isotopes in seawater, which is a function of pH. However while the chemical principles underlying this proxy are well understood, its reliability has previously been questioned, due to the difficulty of boron isotope ($\delta^{11}B$) analysis on foraminferal samples and questions regarding calibrations between $\delta^{11}B$ and pH. This chapter reviews the current state of the $\delta^{11}B$-pH proxy in foraminifera, including the pioneering studies that established this proxy's potential, and the recent work that has improved understanding of boron isotope systematics in foraminifera and applied this tracer to the geological record. The theoretical background of the $\delta^{11}B$-pH proxy is introduced, including an accurate formulation of the boron isotope mass balance equations. Sample preparation and analysis procedures are then reviewed, with discussion of sample cleaning, the potential influence of diagenesis, and the strengths and weaknesses of boron purification by column chromatography versus microsublimation, and analysis by NTIMS versus MC-ICPMS. The systematics of boron isotopes in foraminifera are discussed in detail, including results from benthic and planktic taxa, and models of boron incorporation, fractionation, and biomineralisation. Benthic taxa from the deep ocean have $\delta^{11}B$ within error of borate ion at seawater pH. This is most easily explained by simple incorporation of borate ion at the pH of seawater. Planktic foraminifera have $\delta^{11}B$ close to borate ion, but with minor offsets. These may be driven by physiological influences on the

Electronic supplementary material The online version of this chapter (doi:10.1007/978-3-319-64666-4_5) contains supplementary material, which is available to authorized users.

J.W.B. Rae (✉)
School of Earth and Environmental Sciences,
University of St Andrews, St Andrews, Scotland, UK
e-mail: jwbr@st-andrews.ac.uk

H. Marschall and G. Foster (eds.), *Boron Isotopes*, Advances in Isotope Geochemistry,
https://doi.org/10.1007/978-3-319-64666-4_5

foraminiferal microenvironment; a novel explanation is also suggested for the reduced δ^{11}B-pH sensitivities observed in culture, based on variable calcification rates. Biomineralisation influences on boron isotopes are then explored, addressing the apparently contradictory observations that foraminifera manipulate pH during chamber formation yet their δ^{11}B appears to record the pH of ambient seawater. Potential solutions include the influences of magnesium-removal and carbon concentration, and the possibility that pH elevation is most pronounced during initial chamber formation under favourable environmental conditions. The steps required to reconstruct pH and pCO_2 from δ^{11}B are then reviewed, including the influence of seawater chemistry on boron equilibrium, the evolution of seawater δ^{11}B, and the influence of second carbonate system parameters on δ^{11}B-based reconstructions of pCO_2. Applications of foraminiferal δ^{11}B to the geological record are highlighted, including studies that trace CO_2 storage and release during recent ice ages, and reconstructions of pCO_2 over the Cenozoic. Relevant computer codes and data associated with this article are made available online.

Keywords
Boron isotopes · Foraminifera · CO_2 · Biomineralisation · Proxy

5.1 Introduction

The boron isotope composition of marine carbonates has been widely shown to reflect ocean pH (Vengosh et al. 1991; Hemming and Hanson 1992; Sanyal et al. 1996; Foster 2008; Rae et al. 2011; Henehan et al. 2013). Boron isotope measurements on fossil carbonates thus have the potential to constrain changes in pH and CO_2 over geological time (Pearson and Palmer 2000; Hönisch et al. 2009; Rae et al. 2014; Penman et al. 2014; Greenop et al. 2014; Martínez-Botí et al. 2015a). The shells, or "tests", of foraminifera, which are single-celled protists, provide a convenient host for the δ^{11}B-pH proxy, being widely distributed throughout the world's oceans, relatively well-preserved in marine sediment cores, and having chemistry that closely reflects surrounding seawater conditions (Wefer et al. 1999; Erez 2003). Foraminifera have thus become key agents in geochemical reconstructions of past climates, and boron isotope analyses on foraminifera may be readily compared to tracers of various other conditions determined on the same samples (Katz et al. 2010).

5.1.1 Aqueous Boron Isotope Systematics

The ability of boron isotopes in foraminifera to record seawater pH stems from the acid-base equilibrium between boric acid ($B(OH)_3$) and borate ion ($B(OH)_4^-$):

$$B(OH)_3 + H_2O \rightleftharpoons B(OH)_4^- + H^+. \quad (5.1)$$

The equilibrium constant of this reaction (K_B) is $10^{-8.6}$ (Dickson 1990), giving pK_B of 8.6, close enough to typical ocean pH ($\sim$8) to give large changes in the relative abundance of these molecules as a function of seawater pH (Fig. 5.1a):

$$K_B = \frac{[B(OH)_4^-][H^+]}{[B(OH)_3]}; \quad pK_B \approx 8.6. \quad (5.2)$$

Boron has two stable isotopes, ^{11}B (~80%) and ^{10}B (~20%), and an equilibrium fractionation of 27.2‰ (Klochko et al. 2006) exists between boric acid and borate ion, due to the stronger bonding environment of boron in the trigonal boric acid molecule:

$$\alpha_B = \frac{{}^{11}_{10}R_{B(OH)_3}}{{}^{11}_{10}R_{B(OH)_4^-}} = 1.0272. \quad (5.3)$$

The boron isotope composition of seawater ($\delta^{11}B_{SW}$) is 39.61‰ (Foster et al. 2010). As boron in seawater is overwhelmingly made up of boric acid and borate,[1] the combined boron nuclides within these molecules must give $^{11}B/^{10}B$ equal to that in seawater. Therefore as the abundance of these molecules vary, so too must their isotopic composition (Fig. 5.1b). At low pH, where seawater boron is dominantly present as boric acid, this molecule must have $\delta^{11}B = \delta^{11}B_{SW}$, with an infinitesimal quantity of borate ion offset below this by a function of the fractionation factor:

$$\delta^{11}B_{B(OH)_3} = \delta^{11}B_{B(OH)_4^-} \cdot \alpha_B + \varepsilon_B, \quad (5.4)$$

where $\varepsilon_B = 1000 \cdot (\alpha_B - 1)$. The opposite is true at high pH, while at intermediate pH the isotopic composition of these molecules will vary as a predictable function of pH. This is commonly expressed as the mass balance:

$$\begin{aligned} {}^{11}_{10}R_{SW} \times [B]_{SW} = {}& {}^{11}_{10}R_{B(OH)_3} \times [B(OH)_3] \\ & + {}^{11}_{10}R_{B(OH)_4^-} \times [B(OH)_4^-], \end{aligned} \quad (5.5)$$

from which, rearranging and substituting Eq. (5.4), the following expression for borate isotopic composition as a function of pH can be derived:

$$\delta^{11}B_{B(OH)_4^-} = \frac{\delta^{11}B_{(sw)}[B]_{sw} - \varepsilon_B[B(OH)_3]}{[B(OH)_4^-] + \alpha_B[B(OH)_3]}. \quad (5.6)$$

[1]Minor polynuclear species of aqueous boron exist, such as $B_3O_3(OH)_4^-$, but are only present in negligible quantities at boron concentrations <25 mmol/kg (Su and Suarez 1995), and can thus safely be ignored at seawater concentrations of ~0.4 mmol/kg.

However note that this is an approximation, as mass balance cannot accurately be formulated in terms of isotope ratios. More strictly, we must write the mass balance for each nuclide and then combine these equations to obtain the isotope ratio mass balance. This gives the formula:

$$\begin{aligned} & \frac{{}^{11}_{10}R_{SW} \cdot \left([B(OH)_4^-] + [B(OH)_3]\right)}{{}^{11}_{10}R_{SW} + 1} \\ & = \frac{{}^{11}_{10}R_{B(OH)_4^-} \cdot \alpha_B \cdot [B(OH)_3]}{{}^{11}_{10}R_{B(OH)_4^-} \cdot \alpha_B + 1} \\ & + \frac{{}^{11}_{10}R_{B(OH)_4^-} \cdot [B(OH)_4^-]}{{}^{11}_{10}R_{B(OH)_4^-} + 1}. \end{aligned} \quad (5.7)$$

which can be rearranged and solved (best done by computer; see supplementary code) for the isotopic composition of borate. This is given by the root:

$$\begin{aligned} R_{B(OH)_4^-} = {}& ((H^2 \cdot R_{SW}^2 + 2H^2 \cdot R_{SW} \cdot \alpha_B \\ & + H^2 \cdot \alpha_B^2 + 2H \cdot K_B \cdot R_{SW}^2 \cdot \alpha_B \\ & - 2H \cdot K_B \cdot R_{SW} \cdot \alpha_B^2 \\ & + 8 \cdot H \cdot Kb \cdot R_{SW} \cdot \alpha_B \\ & - 2 \cdot H \cdot K_B \cdot R_{SW} \\ & + 2H \cdot K_B \cdot \alpha_B + K_B^2 \cdot R_{SW}^2 \cdot \alpha_B^2 \\ & + 2K_B^2 \cdot R_{SW} \cdot \alpha_B + K_B^2)^{(1/2)} \\ & - H \cdot \alpha_B - K_B + H \cdot R_{SW} \\ & + K_B \cdot R_{SW} \cdot \alpha_B)/(2 \cdot \alpha_B \cdot (H + K_B)); \end{aligned} \quad (5.8)$$

where R is the $^{11}B/^{10}B$ ratio and H is the hydrogen ion concentration. Equation (5.4) can then be used to calculate the composition of boric acid. The error in calculated boron isotopic compositions resulting from the use of the approximation in Eq. (5.6) compared to the accurate formula in Eq. (5.8) is illustrated in Fig. 5.1c, and may be up to 0.15‰. Matlab codes and an Excel spreadsheet that carry out these calculations are provided in the supplementary online materials.

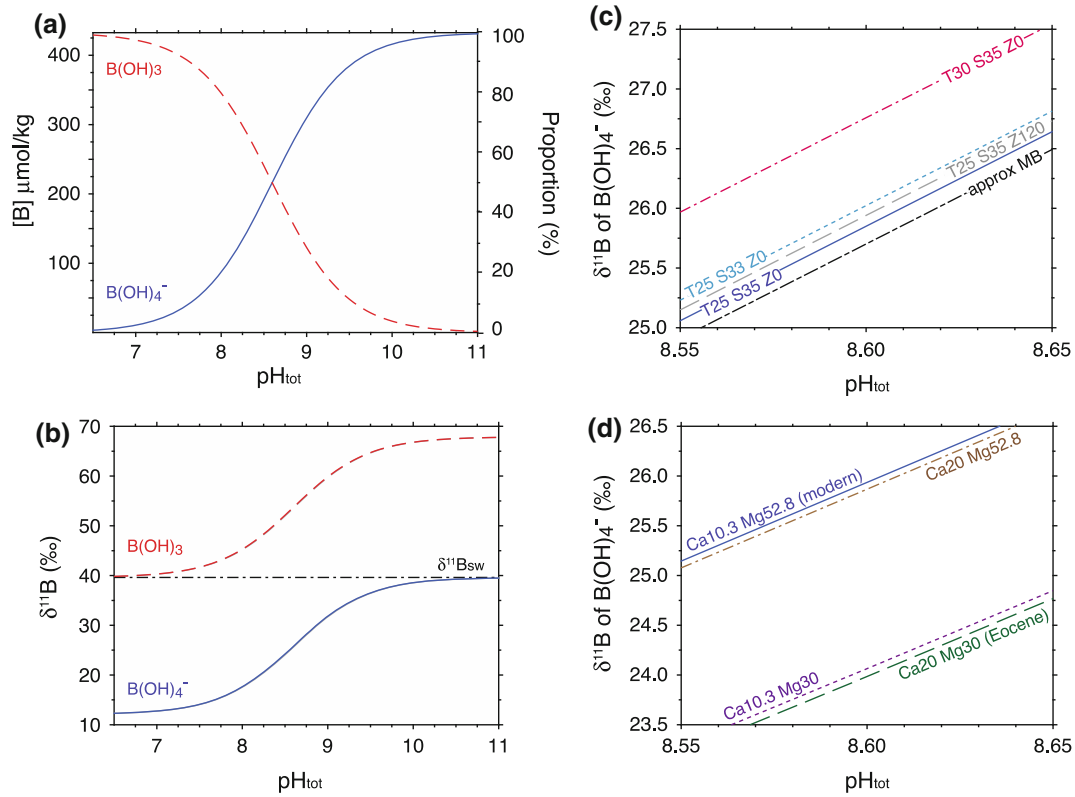

Fig. 5.1 Concentration (**a**) and isotopic composition (**b**) of boric acid and borate ion as a function of seawater pH, at 25 °C, 35 psu, and 0 m depth (Dickson 1990), with modern [Mg] and [Ca], $\delta^{11}B_{SW}$ = 39.61‰ (Foster et al. 2010), and α_B = 27.2‰ (Klochko et al. 2006), calculated using the accurate form of the boron isotope mass balance equation (Eqs. 5.5 and 5.6). **c** Influence of possible changes in temperature, salinity, and pressure at a given site on $\delta^{11}B$ of borate. Note that this plot is focused on the region of pH values close to pK_B, where these influences have greatest sensitivity. Also shown is $\delta^{11}B$ of borate at 25 °C, 35 psu, 0 m depth calculated using the approximate boron isotope mass balance equation (Eqs. 5.5 and 5.6; labeled "approx. MB"). **d** Influence of changes in [Mg] and [Ca] to Eocene values on $\delta^{11}B$ of borate, using the MyAMI model (Hain et al. 2015), are shown individually and together. Code used to make this figure is available in the online materials accompanying this article

5.1.2 The Carbonate δ^{11}B-pH Proxy

Marine carbonates have boron isotopic compositions of ~15–25‰, substantially lower than that of seawater (39.61‰). This is explained by the dominant incorporation of borate ion into growing carbonate (Vengosh et al. 1991; Hemming and Hanson 1992). As the boron isotopic composition of borate varies with pH, so too should $\delta^{11}B$ of marine carbonate.

Early calibrations of boron isotopes in foraminifera showed strong control by pH (Sanyal et al. 1996, 2001), leading to several applications to reconstruct past CO_2 system change and its causes (Sanyal et al. 1995; Pearson and Palmer 2000; Palmer and Pearson 2003). However the reliability of this proxy has been challenged, notably by Pagani et al. (2005a). Concerns with the $\delta^{11}B$-pH proxy have centered on: (1) boron isotope fractionation; (2) mechanisms of boron incorporation into carbonate; (3) vital effects in foraminifera; (4) analytical uncertainties; (5) the evolution of $\delta^{11}B_{SW}$. While several of these topics remain the subject of considerable ongoing research, significant progress has been made on each of these fronts.

Box 1: A quick primer on the ocean carbonate system

The behaviour of boron isotopes in foraminifera discussed in this chapter is intimately linked to the chemistry of CO_2 in seawater, so a brief review of this topic may be helpful. For more detailed treatment see Zeebe and Wolf-Gladow (2001) and Sarmiento and Gruber (2006).

CO_2 reacts with water to form bicarbonate (HCO_3^-) and carbonate ion (CO_3^{2-}):

$$CO_2 + H_2O \overset{K_1}{\Leftrightarrow} H^+ + HCO_3^- \overset{K_2}{\Leftrightarrow} 2H^+ + CO_3^{2-}$$

where K_1 and K_2 are the first and second dissociation constants for carbonic acid, and have values of $\sim 10^{-6}$ and $\sim 10^{-9}$ respectively (varying with temperature, salinity, pressure, and major ion chemistry).

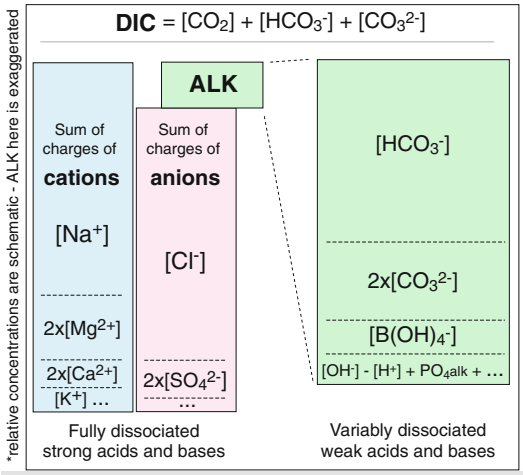

pH (and thus $\delta^{11}B$ of borate) is a sensitive tracer of the equilibrium state of this acid-base system. However this state is actually controlled by the balance between the master variables alkalinity (ALK) and dissolved inorganic carbon (DIC). DIC is simply the total concentration of inorganic carbon molecules. ALK is analytically defined as the number of moles of strong acid required to drive seawater to the equivalence point of bicarbonate. More intuitively, ALK is equivalent to the charge imbalance between strong bases and strong acids in seawater (see inset figure based on Broecker 2005). The requirement for charge balance is taken up largely by variable dissociation of weak acids and bases, predominantly those of CO_2 and boron.

Therefore if alkalinity is large and the pool of DIC to balance it is relatively small, the carbonate system must be pulled toward doubly charged CO_3^{2-}; vice versa, if a large pool of DIC exists but alkalinity is small, much of the DIC must be present as uncharged CO_2. pCO_2, $[CO_3^{2-}]$, pH (and $[B(OH)_4^-]$) are thus primarily controlled by the balance of ALK and DIC, and as a result are tightly coupled and closely traced by $\delta^{11}B$ of borate. This is well illustrated by a ALK-DIC contour plot (inset figure, plotted for 25 °C, 35 psu, and 0 m water depth).

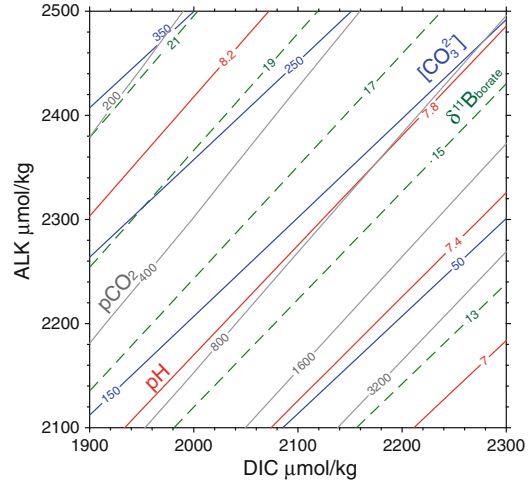

A final important concept is calcium carbonate mineral saturation (Ω):

$$\Omega = \frac{[Ca^{2+}] \times [CO_3^-]}{K_{sp}}$$

where K_{sp} is the equilibrium solubility product, $\sim 10^{-6.4}$ for calcite and $\sim 10^{-6.2}$ for aragonite in the surface ocean. Undersaturated conditions correspond to $\Omega < 1$, supersaturated conditions to $\Omega > 1$. $\Omega_{calcite}$ ranges from ~4–6 in most of the modern surface ocean, dominantly as a function of $[CO_3^{2-}]$, and decreases to <1 at depth.

5.2 Methods of Boron Isotope Analysis in Foraminifera

The analysis of boron isotopes is discussed in detail by Foster et al. (2013) for carbonates, and in Chap. 2 of this volume for a broad range of natural samples. Below I provide a brief overview of the specifics of $\delta^{11}B$ analysis of foraminifera, which is challenging due to the small sample sizes and complex matrix involved, and has been a topic of considerable discussion (Ni et al. 2010; Foster et al. 2013; Farmer et al. 2016).

5.2.1 Samples

5.2.1.1 Sample Size and Preparation

Foraminiferal samples are taken from ocean sediment cores, plankton tows, and culture experiments. For solution analyses between ~2 and 20 ng boron are typically used. Boron concentrations and shell masses vary considerably between different species of foraminifera (Yu and Elderfield 2007; Henehan et al. 2016), dictating the number of foraminifera required: for low mass (5–20 μg) low B/Ca (40–60 μmol/mol) planktic species such as *G. bulloides* and *N. pachyderma*, ~400 specimens are typically required; for bulkier (10–30 μg) or higher B/Ca (80–120 μmol/mol) planktic species such as *T. sacculifer* and *G. ruber*, ~100 specimens are required; for higher B/Ca epifaunal benthic species such as *C. wuellerstorfi* and *C. mundulus* (~30–100 μg; 100–250 μmol/mol) it is possible to analyze ~2–20 specimens. Note that analytical uncertainty increases as sample sizes are reduced (Rae et al. 2011).

For sediment core samples, standard 10 cm^3 volumes of pelagic sediment are often sufficient, though this may vary considerably depending on setting. As with any foraminifera-based work, sediment disaggregation and sieving is required; detergents and disaggregation agents (Feldmeijer et al. 2013) may have high levels of boron and should be avoided.

5.2.1.2 Preservation and Diagenesis

Preservation state of foraminifera is not currently thought to exert major influence on boron isotope ratios. For instance, no change in $\delta^{11}B$ with partial dissolution is seen in recent *G ruber* (Ni et al. 2007; Seki et al. 2010; Henehan et al. 2013) or *C. wuellerstorfi* (Rae et al. 2011). Although changes in $\delta^{11}B$ have been noted with partial dissolution in recent *T. sacculifer*, this is thought to be due to the presence of dissolution resistant and anomalously low-$\delta^{11}B$ gametogenic calcite in this species (Hönisch and Hemming 2004; Ni et al. 2007; Seki et al. 2010).

Edgar et al. (2015) show similar $\delta^{11}B$ between well-preserved "glassy" and partially recrystallized "frosty" planktic foraminifera of Eocene age, despite lower B/Ca in the recrystallized samples. This may result from only partial exchange with pore waters during foraminiferal recrystalisation and from low partitioning of boron into inorganically (re)precipitated calcite (Uchikawa et al. 2015) compared to the original foraminiferal carbonate, especially under low-pH (and thus low borate) conditions (Edgar et al. 2015). Mass balance may thus help minimize the influence of diagensis on foraminiferal $\delta^{11}B$.

5.2.2 Cleaning of Foraminiferal Samples

Samples of foraminifera for $\delta^{11}B$ analysis are typically subjected to physical and chemical cleaning, of the type developed for trace element determinations (Boyle 1981; Barker et al. 2003; Ni et al. 2007). This involves gentle crushing to open chambers, repeat ultrasonication in deionized water to remove clays, and oxidation of organic matter in bleach or buffered hydrogen peroxide. Extensive tests of the influence of cleaning on B/Ca ratios suggest that reductive cleaning, commonly employed for Cd/Ca, has little effect on B/Ca, but can result in substantial loss of shell material (Yu et al. 2007). This step is thus typically omitted when cleaning foraminifera for $\delta^{11}B$ (though may still be used if

certain other trace element analyses on the same sample are required). Note that given the high contents of organic matter in cultured and towed foraminifera, these samples are typically subjected to a more thorough oxidative cleaning (Russell et al. 2004; Henehan et al. 2013). To check for sample cleanliness and obtain complementary proxy data, several laboratories analyse trace element ratios (e.g. Al/Ca) on aliquots of the same samples prior to boron isotope analyses. No strict cut-off value for contamination exists, as the boron to aluminium ratio and the boron isotope composition of the leachate will vary between samples, but samples with Al/Ca of a few hundred μmol/mol or more may be treated with suspicion (see also Deyhle and Kopf 2004).

5.2.3 Chemical Purification

Chemical purification of boron from the sample matrix is required prior to analysis by Multi-Collector Inductively-Coupled-Plasma Mass Spectrometry (MC-ICPMS; see Wei et al. 2014). Some Negative Thermal Ionisation Mass Spectrometry (NTIMS) methods also employ chemical purification, whereas others load samples in their dissolved carbonate matrix (compare Duke and Lamont methods in Foster et al. (2013) and see discussion in Farmer et al. 2016).

5.2.3.1 Column Chromatography

Boron purification is typically carried out using column chromatography, taking advantage of the Amberlite 743 boron-specific resin (Kiss 1988; Lemarchand et al. 2002). Dissolved samples are buffered to elevate pH, which allows borate to complex with the resin's N-methyl-glucamine groups (Yoshimura et al. 1998). $CaCO_3$ matrix is then removed using deionized water, and boron is eluted using dilute acid. Some laboratories use a cation column to reduce major ion concentrations prior to Amberlite purification (Paris et al. 2010a; Trotter et al. 2011); and see Paris and Duke methods in Foster et al. 2013). As boron is volatile in acidic conditions (Gaillardet et al. 2001) it is not possible to pre-concentrate samples by evaporation, so column volumes must be minimized to concentrate boron for analysis. The column chromatography approach is common in isotope geochemistry and can provide data with reproducibility of ~0.2‰ (2SD; e.g. Rae et al. 2011). However the relatively long exposure time of samples purified by this technique requires laboratory contamination ("blank") to be carefully controlled. This likely accounts for poor inter-laboratory reproducibility between MC-ICPMS techniques at small sample sizes (see discussion in Foster et al. 2013). Control of laboratory blank is a unique challenge for boron, due to the common use of boro-silicate fibers in HEPA filters, lab insulation, and fire-retardants (Rosner et al. 2005). However as boron contamination is also a problem for the semi-conductor industry, boron-free alternatives are available, allowing total procedural blanks to be kept to <100 pg under carefully controlled conditions (Wang et al. 2010; Rae et al. 2011).

5.2.3.2 Microsubliation

Boron purification has also been carried out by "micro-sublimation" (Gaillardet et al. 2001; Wang et al. 2010; Misra et al. 2014). This takes advantage of the volatility of boron to evaporate it from the sample matrix. The dissolved sample is loaded onto the upturned lid of a Teflon beaker, which is then closed and placed on a hotplate, allowing boron to evaporate from the matrix and condense along with water in the beaker's upturned base. This method has the advantage of being totally enclosed, minimizing contamination. Microsublimation has yielded promising results for solution standards, seawater, and multiple aliquots of dissolved carbonate samples (Gaillardet et al. 2001; Wang et al. 2010; Misra et al. 2014). However results on foraminifera are more limited and, to date, show poorer reproducibility; for instance Misra et al. (2014) show that multiple solid splits of a foraminiferal sample have variability of ~1.7‰ (2SD). This is significantly larger than replicate aliquots of a single solution by this method (~0.5‰, 2SD), and cannot be attributed to sample heterogeneity, as the same levels of scatter are seen in subsamples of 25 and 50

foraminiferal tests (Misra et al. 2014). This may suggest variable mass fractionation during boron evaporation as a function of subtle differences in sample matrix.

5.2.4 Mass Spectrometry

5.2.4.1 NTIMS

The pioneering early work on boron isotopes in foraminifera was carried out by Negative Thermal Ionisation Mass Spectrometry (Hemming and Hanson 1994; Sanyal et al. 1995; Pearson and Palmer 2000). By switching polarity from typical positive TIMS and analyzing boron as BO_2^- beams instead of $Cs_2B_2^+$, sample sizes were reduced to levels permitting analysis of small foraminiferal samples (Hemming and Hanson 1994). As described in greater detail in Chap. 2, the carbonate matrix promotes ionization of boron, so dissolved foraminifera are typically loaded directly onto filaments with no further purification (Kasemann et al. 2009; Farmer et al. 2016). However this sensitivity to matrix has the potential to introduce inaccuracies, with NTIMS analyses deviating from MC-ICPMS values in samples with low boron/matrix ratios (see inter-laboratory comparison by Foster et al. (2013) and intra-laboratory comparison by Farmer et al. 2016), though the exact cause of these offsets remains unknown.

5.2.4.2 MC-ICPMS

MC-ICPMS is increasingly used for analysis of boron isotopes on marine carbonates. As described above and in Chap. 2, this technique requires careful separation of boron from the carbonate matrix, and has further challenges including memory effects in the sample introduction system due to boron's volatility (Al-Ammar et al. 2000), large mass bias (~15% per amu) requiring stable-enough conditions for accurate correction by sample-standard bracketing (Foster 2008), and relatively low sensitivity (~10 mV/ppb using a 50 µl/min nebuliser). Recent inter-laboratory comparison shows good agreement (~0.5‰ 2SD) between MC-ICPMS analyses for relatively large samples (Foster et al. 2013; Gutjahr et al. 2014). However reproducibility is notably poorer for smaller samples, of the size typically used in foraminiferal analyses (Foster et al. 2013), highlighting the need for careful control of laboratory blank.

5.2.4.3 In Situ Analysis

Laser-Ablation MC-ICPMS (LA-MC-ICPMS) and Secondary Ionisation Mass Spectrometry (SIMS) can be used to make in situ analyses of $\delta^{11}B$ in foraminifera (Rollion-Bard and Erez 2010; Fietzke et al. 2010; Kaczmarek et al. 2015). Until recently, the precision of these methods has been relatively low, due to low count rates. However recent technical developments, along with pooling of multiple spots have considerably improved LA-MC-ICPMS precision (Fietzke et al. 2015; Sadekov et al. 2016). Accurate correction for mass bias in situ analyses requires homogenous and carefully characterized standards, and matrix matching is important for SIMS (Kasemann et al. 2009), though less so for LA-MC-ICPMS (Fietzke et al. 2015). While in situ analysis is unlikely to replace bulk/solution techniques for generating foraminiferal $\delta^{11}B$ records, it may provide valuable insights into the distribution of boron isotopes within foraminiferal carbonate, and the statistical spread of $\delta^{11}B$ values of individuals within a sample population (Rollion-Bard and Erez 2010; Kaczmarek et al. 2015; Sadekov et al. 2016).

5.3 Boron Isotope Systematics in Modern Foraminifera

A particular attraction of the $\delta^{11}B$-pH proxy is its underlying chemical framework: pH controls $\delta^{11}B$ of borate, and as borate is thought to be incorporated in foraminifera, foraminiferal $\delta^{11}B$ should track pH. However it is possible that equilibrium or kinetic isotopic fractionations occur on boron incorporation into carbonate, and/or that foraminiferal physiology may impart further offsets from inorganic systematics (known as "vital effects"). Thus it is crucial to test the relationship between $\delta^{11}B$ of borate,

calculated from measured seawater pH, and foraminiferal $\delta^{11}B$. This has been achieved with measurements of natural modern samples taken from sediment core-tops, plankton tow nets and sediment traps, and using culturing experiments, where foraminifera are taken from the wild and grown in controlled laboratory conditions over a range of pH.

As $\delta^{11}B$ proxy calibration studies aim to test the relationship between $\delta^{11}B$ in foraminifera and borate—on which this proxy is based—presenting calibration data on cross-plots of foram $\delta^{11}B$ versus $\delta^{11}B$ of borate is recommended. This also has the advantage over presentation on $\delta^{11}B$-pH figures that different environmental conditions may be readily plotted together, whereas $\delta^{11}B$-pH figures may only be constructed for a single set of environmental conditions (T, S, P, and resulting K_B). However given that several previous studies have shown calibration data on $\delta^{11}B$-pH figures, these are also shown here for reference, with data plotted at the pH of the original growth conditions and $\delta^{11}B$ re-calculated for standard surface water conditions of 25 °C and 35 psu. This is achieved by applying the offset between foraminiferal and borate $\delta^{11}B$ found at the original growth conditions to the $\delta^{11}B$ of borate calculated with K_B for 25 °C, 35 psu, and 0 m depth, at the original growth pH, i.e.

1. calculate $\delta^{11}B$ offset at in situ conditions: $\Delta\delta^{11}B = \delta^{11}B_{foram} - \delta^{11}B_{borate\text{-}in\ situ}$;
2. calculate K_B at the T, S, P conditions of the desired pH-$\delta^{11}B$ plot, using Eq. (5.11) (and 5.12 and 5.13 if plotting at non-zero water depths);
3. calculate $\delta^{11}B$ of borate for the desired plot conditions using Eq. (5.8), with K_B from step 2 above, and pH from the original measurement at in situ conditions;
4. apply the $\delta^{11}B$ offset from step 1 to $\delta^{11}B$ of borate calculated in step 3, to give the adjusted foram $\delta^{11}B$: $\delta^{11}B_{foram\text{-}adjusted} = \delta^{11}B_{borate\text{-}plot} + \Delta\delta^{11}B$.

Other approaches to this adjustment are possible (for instance using pH rather than $\delta^{11}B$ offsets), but the assumptions and steps in the approach above are the most straightforward.

Boron isotope data on modern foraminifera are discussed below, from deep sea calcitic benthic, planktic, and other benthic foraminifera in turn. The implications of these data for $\delta^{11}B$-pH systematics are then synthesized, including modes of boron incorporation into foraminiferal carbonate, isotopic fractionation and physiological influences, and constraints on pH during biomineralisation.

5.3.1 Results of Boron Isotope Calibration Studies on Modern Foraminifera

5.3.1.1 Deep Sea Benthic Foraminifera —A Model System?

The low-Mg calcite hyaline benthic foraminifera found in deep ocean environments provide a useful starting point for assessing foraminiferal boron isotope systematics. This grouping includes a wide range of genera, lacks symbionts, is thought to have relatively low metabolic rate, and inhabits stable deep-sea environments that span a wide range of conditions (pH, T, S, P, ΔCO_3^{2-} etc.).

Deep sea benthic foraminifera appear to record the $\delta^{11}B$ of borate ion—and thus pH—of the surrounding water with little or no modification. This is most readily demonstrated for the epifaunal taxa *Cibicides* and *Planulina* (Rae et al. 2011; Yu et al. 2010), which inhabit the sediment surface and thus have the closest association with bottom water conditions (Figs. 5.2 and 5.3). In a set of 45 foraminiferal $\delta^{11}B$ samples spanning 17 different sites in the Atlantic, *C. wuellerstorfi, C. mundulus, C. lobatus, C. ungerianus, and P. ariminensis* all have $\delta^{11}B$ that closely matches $\delta^{11}B$ of borate at bottom water pH (Rae et al. 2011). There are no systematic differences in $\delta^{11}B$ values with different foraminiferal test size nor between species (Rae et al. 2011). *C. wuellerstorfi* appears to track bottom water pH conditions with least scatter, as previously observed for other geochemical tracers ($\delta^{13}C$, $\delta^{18}O$, element/calcium ratios), likely due to its

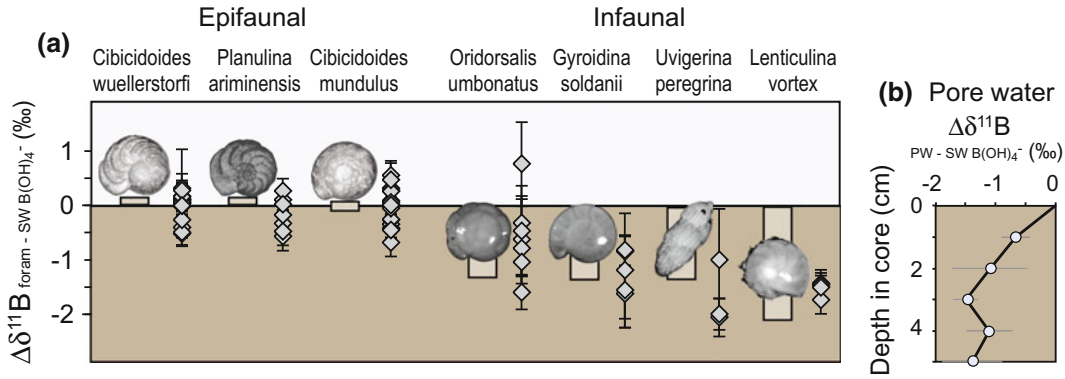

Fig. 5.2 **a** Offsets between $\delta^{11}B$ measured in core-top benthic foraminifera from deep ocean sediment cores and $\delta^{11}B$ of borate ion calculated for overlying seawater (Rae et al. 2011). Uncertainties are equivalent to 2SD on repeat analyses. Calcite epifaunal foraminifera have $\delta^{11}B$ within error of seawater borate, while infaunal foraminifera are offset below bottom water by up to 2‰. **b** Offset between $\delta^{11}B$ of borate in bottom water and pore waters, averaged from 3 sediment cores from the Namibian margin. Pore water $\delta^{11}B$ of borate values are calculated from measured pH and $\delta^{11}B$ of pore water (Rae et al. 2011); the mean and 2SE of $\delta^{11}B$ of borate in each of the top 5 cm is shown for three nearby cores. These offsets are similar to those seen between bottom water and infaunal benthic foraminifera (some of which were taken from these cores), suggesting that these species record $\delta^{11}B$ of borate in their ambient pore water conditions

elevated epifaunal habitat (Lutze and Thiel 1987).

Infaunal benthic foraminifera also appear to record $\delta^{11}B$ of borate, but at conditions reflecting their pore water environment (Fig. 5.2). Infaunal species analysed to date include *C. robertsonianus, Oridorsalis umbonatus, Gyroidina soldanii, Uvigerina peregrine, Melonis zaandamae, Ammonia beccarii,* and *Lenticulina vortex*, inhabiting the top few cm of deep sea sediment. Infaunal foraminifera have $\delta^{11}B$ up to 2‰ lower than $\delta^{11}B$ of borate in bottom waters. However pH may be lowered in pore waters by oxidation of organic matter, and $\delta^{11}B$ of pore water itself may be lowered by interaction with light boron from clays, carbonate, opal, and organic matter (Rae et al. 2011). These factors combine to decrease $\delta^{11}B$ of borate by around −0.5 to −2.0‰ in the top 5 cm of pore waters compared to overlying bottom waters (Fig. 5.2b), similar to the $\delta^{11}B$ offsets seen in infaunal benthic foraminifera (Fig. 5.2a). More detailed comparison of pore-water chemistry and infaunal $\delta^{11}B$ is limited by knowledge of sedimentary habitat depths; nonetheless, the most simple explanation of $\delta^{11}B$ in infaunal foraminifera is that it follows the same systematics as in epifaunal species, incorporating borate ion but at the conditions of the surrounding pore water (Corliss 1985).

The close match between $\delta^{11}B$ of benthic foraminifera and $\delta^{11}B$ of borate at the pH of the surrounding water, across a wide range of environmental conditions and different taxa, provides support for simple models of $\delta^{11}B$-pH proxy systematics (e.g. Hemming and Hanson 1992 and see Sect. 3.2.1).

5.3.1.2 Planktic Foraminifera—Key Proxy Carriers

Planktic foraminifera have been the focus of much of the development work on foraminiferal boron isotopes, due to the importance of surface ocean $\delta^{11}B$-derived pH records in studies of past atmospheric CO_2. Modern planktic foraminifera evolved from benthic species (Hemleben et al. 2012), and have relatively simple low-Mg calcite tests compared to the variety found in benthic taxa. However despite their low taxonomic diversity, planktic foraminifera span a wide range of ecological niches and lifestyles, ranging from shallow-dwelling taxa with photosynthetic symbionts, to deep-dwelling taxa lacking symbionts.

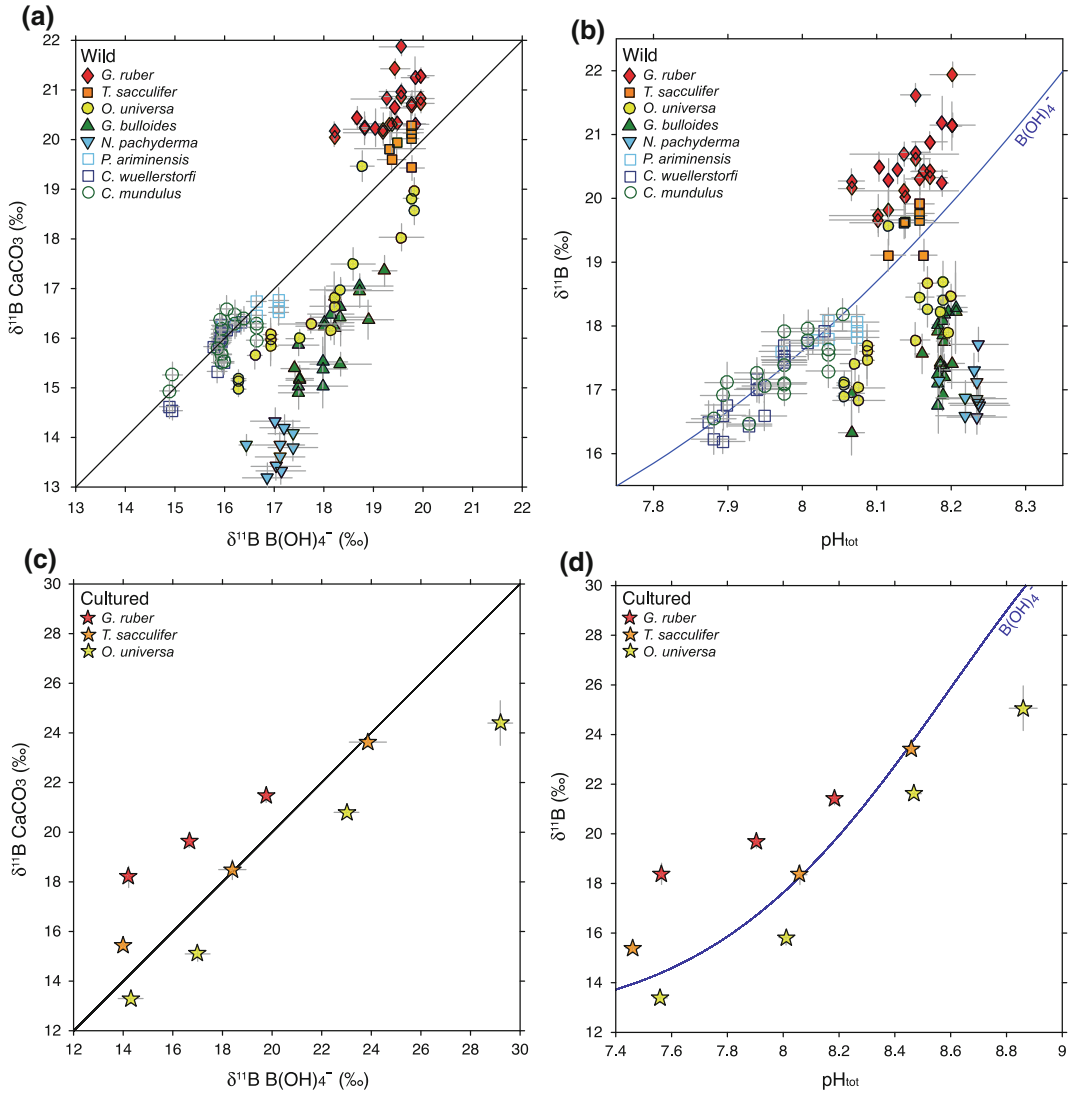

Fig. 5.3 **a** Boron isotope data from modern planktic and benthic foraminifera from core-tops and plankton tows, compared to $\delta^{11}B$ of borate calculated from carbonate system data in ambient seawater. **b** Boron isotope data from panel (**a**) re-plotted at 25 °C, 35 psu, and 0 m water depth, compared to pH from carbonate system data in ambient seawater. To re-plot boron isotope data, the $\delta^{11}B$ offsets between foraminifera and borate ion found at the original growth conditions are added to the $\delta^{11}B$ of borate calculated with pKb for 25 °C, 35 psu, and 0 m depth at the original growth pH (see main text Sect. 5.3). **c**, **d** are equivalent to (**a**) and (**b**) but for cultured planktic foraminifera. Wild planktics: *G. ruber* data are from Henehan et al. (2013) and Foster (2008), *T. sacculifer* (formerly known as *G. sacculifer*) data are from Foster (2008) and Martínez-Botí et al. (2015b), *O. universa* data are from Henehan et al. (2016), *G. bulloides* data are from Martínez-Botí et al. (2015b), *N. pachyderma* data are from Yu et al. (2013). Wild benthics: *P. ariminensis*, *C. wuellerstorfi*, and *C. mundulus* data are from Rae et al. (2011). Cultured planktics: *G. ruber* data are from Henehan et al. (2013), *O. universa* data are from Sanyal et al. (1996), with a −3.3‰ offset to account for interlaboratory bias (Henehan et al. 2016), and *T. sacculifer* data are from Sanyal et al. (2001), with a −5.3‰ offset to account for interlaboratory bias (Foster et al. 2012). Uncertainties are 2σ and taken from original publications. Code and data used to make this figure are available in the online materials accompanying this article

The life span of most planktic species is relatively short (weeks to months), so metabolic rates are high: compared to benthic foraminifera, planktics tend to live fast and die young. Some species have preferences for certain seasons, and some may migrate through different water depths during their life cycle. However individual species tend to occupy a relatively limited set of environmental (e.g. pH and temperature) conditions (Bijma et al. 1990). These factors, along with limited depth and seasonally-resolved water-column pH data, may complicate proxy calibration in planktic foraminifera from the wild (e.g. core-tops, tows, sediment traps). Culturing experiments have thus been employed in $\delta^{11}B$ calibrations to provide an expanded pH range with controlled environmental conditions, but do not necessarily provide analogous conditions to the open ocean.

Boron isotope data from all planktic foraminifera analysed to date lie within a few permil of $\delta^{11}B$ of borate and show sensitivity to seawater pH (Fig. 5.3). However while $\delta^{11}B$ values lie close to $\delta^{11}B$ of borate (compared to $\delta^{11}B$ of seawater or boric acid), there are notable offsets. Species lacking photosynthetic symbionts (including *G. bulloides* and *N. pachyderma*) have $\delta^{11}B$ below that of borate ion (i.e. an offset to lower pH), while symbiont-bearing species (e.g. *G. ruber* and *T. sacculifer*) tend to have $\delta^{11}B$ above borate at seawater pH (i.e. an offset to higher pH; Hönisch et al. 2003).

These offsets may be explained by the physiological influences of photosynthesis, respiration, and calcification on the foraminiferal microenvironment (Zeebe et al. 2003; Fig. 5.4a). Photosynthesis draws down CO_2, raising microenvironmental pH, while respiration releases CO_2, lowering pH (Wolf-Gladrow et al. 1999). Calcification draws down two moles of alkalinity (via Ca^{2+}) per one mole of dissolved inorganic carbon (either as HCO_3^- or CO_3^{2-}), resulting in a net lowering of pH (see Box 1 for a quick review of carbonate chemistry). The influence of these processes on the microenvironment of planktic foraminifera has been demonstrated using microelectrodes (Rink et al. 1998; Köhler-Rink and Kühl 2000), which reveal pronounced gradients in pH and O_2 in the diffusive boundary layer surrounding planktic foraminifera. Culturing studies demonstrate that these processes are reflected in boron isotope composition (Hönisch et al. 2003), with an increase in $\delta^{11}B$ of *O. universa* grown at increasing light levels, due to enhanced photosymbiont activity. These offsets have also been reproduced in a diffusion-reaction model of the foraminiferal microenvironment (Zeebe et al. 2003; and see further discussion below). Physiological alteration of foraminiferal microenvironment may also account for the influence of size on $\delta^{11}B$ in symbiont-bearing planktic foraminifera (Zeebe et al. 2003). Increases in $\delta^{11}B$ with shell size are seen in *G. ruber* and *T. sacculifer* (Henehan et al. 2013; Ni et al. 2007; Hönisch and Hemming 2004), which may result from documented increases in photosynthetic rates relative to respiration with increasing test size (Lombard et al. 2010; Hemleben and Bijma 1994).

Given the influence of physiological processes on planktic foraminiferal $\delta^{11}B$, it is crucial for proxy calibration to test how these are realized in modern ocean settings. This is well-illustrated by recent open ocean $\delta^{11}B$ data from *O. universa* (Henehan et al. 2016), which are offset below $\delta^{11}B$ of borate at seawater pH, despite the presence of dinoflagellate symbionts. This may be explained by the fact that *O. universa* tends to inhabit water depths where light attenuation may limit photosynthetic activity (Morard et al. 2009; Jorgensen et al. 1985). Respiration and calcification thus exert a greater net influence than photosynthesis at the habitat depth of *O. universa*, leading to an offset to lower $\delta^{11}B$ and pH. Indeed Hönisch et al. (2003) note that their culture experiments that used low light levels lie closest to their *O. universa* data from plankton tows (though not core-tops).

Early culture work (Sanyal et al. 1996) suggested that $\delta^{11}B$ in *O. universa* showed a lower sensitivity to pH than $\delta^{11}B$ of borate (Fig. 5.3c, d). However this is not seen in the wild data of Henehan et al. (2016), which closely follow $\delta^{11}B$ of borate with a small constant offset (see further discussion in Sect. 3.2.2). Indeed despite the

influence of physiology on planktic foraminiferal $\delta^{11}B$, Henehan et al. (2016)'s open ocean *O. universa* data—from plankton tows and core tops—demonstrate that these vital effects may be remarkably stable, or closely coupled, over a wide range of environmental conditions.

5.3.1.3 Other Benthic Foraminifera—Enigmatic Signals in High-Mg Calcite and Aragonite

Large, high-Mg calcite, reef-dwelling benthic foraminifera of the genus *Amphistegina* are commonly used in culture studies of biomineralisation, being relatively robust to environmental change, easy to collect, and large enough to image effectively. However boron isotope data on *Amphistegina* from different studies are currently somewhat conflicting. While Rollion-Bard and Erez (2010)'s SIMS data, when averaged, give bulk $\delta^{11}B$ values lying ~5–12‰ above $\delta^{11}B$ borate, Kaczmarek et al. (2015)'s recent laser ablation data range from values ~2‰ above borate to ~7‰ below. Kaczmarek et al. (2015) also find a range of ~6‰ between different specimens cultured under the same environmental conditions, with the lowest $\delta^{11}B$ values in these specimens lying below the lower limit for $\delta^{11}B$ of borate ion.

The cause of these offsets between specimens and studies is currently unknown. However the range of $\delta^{11}B$ in specimens taken from the same environmental conditions suggests strong but variable internal control of $\delta^{11}B$ by individual foraminifera of this species under these conditions. Internal control of $\delta^{11}B$ in Amphistegina was also suggested by Rollion-Bard and Erez (2010), who found a notable change in the spread of $\delta^{11}B$ values from individual SIMS spots in a given specimen as a function of pH (see Sect. 3.2.3 on Biomineralisation).

Enigmatic boron isotope results have also been obtained from the only common modern aragonitic foraminifera, *Hoeglundina elegans*. Indeed the life style of this species is in itself an enigma, being widely distributed in the deep ocean at depths and conditions where aragonite is highly undersaturated. Boron isotope values from this epifaunal species lie below ambient borate by ~0.5–3.5‰ (Rae et al. 2011), notably different to low-Mg epifaunal benthic foraminifera. Indeed the lowest $\delta^{11}B$ values from this species (11.97‰; Rae et al. 2011) lie below the lower limit of seawater borate ion, suggesting further isotopic fractionation during biomineralisation in this species.

5.3.2 Discussion of Boron Isotope Calibration on Modern Foraminifera

The synthesis of boron isotope data on modern foraminifera presented above provides a basis to re-evaluate the assumptions underlying the $\delta^{11}B$-pH proxy, and provides powerful constraints on models of calcification.

5.3.2.1 Boron Incorporation in Foraminifera

A key assumption in the use of boron isotopes in marine carbonates to reconstruct pH is that only borate ion is incorporated into carbonate (for more detailed discussion see Chap. 3 by Branson and recent paper by Balan et al. 2016). Given the physiological influences on planktic foraminiferal $\delta^{11}B$, the deep sea benthic foraminifera provide a useful model system to test this assumption. The close match between epifaunal benthic $\delta^{11}B$ and $\delta^{11}B$ of borate (Figs. 5.2 and 5.3) strongly supports the exclusive incorporation of borate ion from seawater into foraminiferal carbonate: incorporation of just 4% boric acid would offset benthic $\delta^{11}B$ from borate ion by more than 1‰, in contrast with the close match observed. Indeed across a wide range of life styles and environments, and despite physiological influences, almost all foraminiferal $\delta^{11}B$ data lie relatively close to $\delta^{11}B$ of borate, and are substantially below $\delta^{11}B$ of seawater or boric acid.

Although NMR data have shown the presence of both tetrahedrally and trigonally coordinated boron in biogenic carbonates (Sen et al. 1994; Klochko et al. 2009; Rollion-Bard et al. 2011; Noireaux et al. 2015; Mavromatis et al. 2015), this does not necessarily reflect the coordination of the molecule incorporated from solution

(Klochko et al. 2009; Balan et al. 2016). Indeed some re-coordination of tetrahedral borate is to be expected upon incorporation into trigonal calcite (Hemming et al. 1995; Klochko et al. 2009), with recent quantum mechanical modelling showing that boron is structurally substituted for carbonate groups in the calcite lattice, being found as partially deprotonated trigonal $BO_2(OH)^{2-}$ and minor $B(OH)_4^-$ (Balan et al. 2016). Although under equilibrium conditions isotopic fractionation may be expected between borate and $BO_2(OH)^{2-}$, if this re-coordination occurs during incorporation without further exchange with seawater, it may not be expressed. Indeed recent synchrotron work (Branson et al. 2015) suggests that boron may be exclusively present in trigonal form in calcitic benthic foraminifera. If this trigonal boron were to reflect boric acid incorporation, foraminiferal $\delta^{11}B$ values should lie ~28‰ above borate. However $\delta^{11}B$ data on these samples lie within a few ‰ of $\delta^{11}B$ of borate ion (Kaczmarek et al. 2015), supporting exclusive addition of borate ion to growing calcite, with re-coordination to trigonal form upon incorporation into foraminiferal calcite with no further isotopic exchange (Hemming and Hanson 1992).

Although some recent experimental work has suggested that boric acid may be incorporated into inorganically precipitated calcites, results from different studies are conflicting. Based on boron concentration data, Uchikawa et al. (2015) suggest that partitioning of boron into calcite is best described in terms using total boron in solution rather than borate ion, especially at high precipitation rates. However preliminary $\delta^{11}B$ data on these same precipitates lie close to borate ion (Farmer et al. 2015), inconsistent with substantial incorporation of boric acid. Noireaux et al. (2015) provide $\delta^{11}B$ data on inorganic aragonite and calcite precipitates (as used in Mavromatis et al. 2015). While Noireaux et al. (2015)'s aragonites have $\delta^{11}B$ within error of borate ion, the calcites have $\delta^{11}B$ up to ~10‰ higher than borate, and these authors suggest incorporation of boric acid may account for this offset. However in a separate study, Kaczmarek et al. (2016) give $\delta^{11}B$ values for inorganic calcite precipitates within 1.5‰ of borate ion, supporting the predominant incorporation of borate. Further work is required to reconcile these conflicting results and this will doubtless lead to improved understanding of the fundamental mechanisms of boron incorporation into carbonate (Balan et al. 2016). However it should be noted that inorganic experiments do not provide a perfect analogue to precipitation of calcite by foraminifera, and that foraminiferal $\delta^{11}B$ data are currently most easily explained by exclusive incorporation of borate ion at pH close to that in surrounding seawater.

5.3.2.2 Boron Isotope Fractionation in Foraminifera

The boron isotope fractionation factor between boric acid and borate ion was, for a long time, poorly constrained (see further discussion in Chap. 8). Early studies frequently used a value of 1.0194, based on calculations by Kakihana and Kotaka (1977) using vibrational frequency data from Kotaka and Kakihana (1977). However it was later shown that a major vibrational frequency mode had been improperly assigned in these calculations (Rustad and Bylaska 2007), and recalculation using various methods yields higher values, though with considerable range (~1.020–1.050; Oi 2000; Liu and Tossell 2005; Zeebe 2005). Experimental determination of the fractionation factor was thus crucial. Klochko et al. (2006) achieved this with an elegant experiment that takes advantage of the fact that pure ^{10}B boric acid and pure ^{11}B boric acid have subtly different dissociation constants, which can be linked to the fractionation factor. This yields an isotopic fractionation of 1.0272 ± 0.0006 (95% confidence) between borate and boric acid in seawater, which has been widely adopted. This has recently been corroborated using an independent experimental set-up, based on separation of boric acid from borate ion (and associated ion pairs) using reverse osmosis, and isotopic measurement of these solutions (Nir et al. 2015). This yields a value of 1.0260 ± 0.001, within error of the Klochko et al. (2006) value.

Although the aqueous fractionation factor is now well constrained, there has been continued

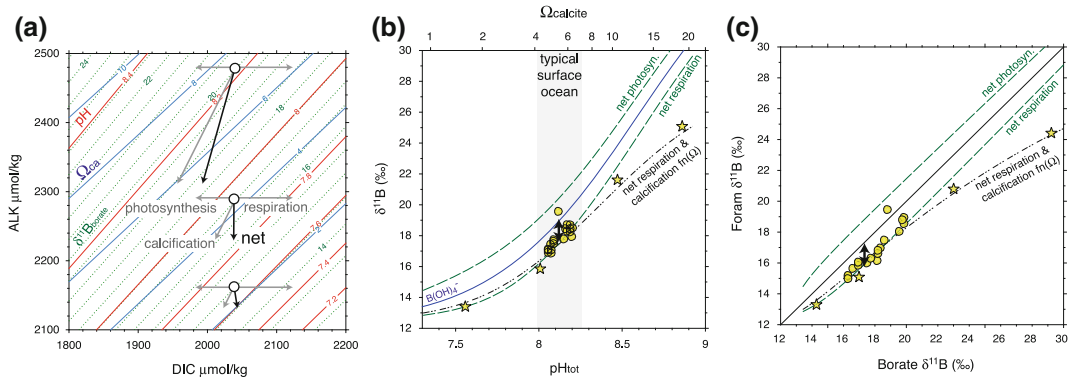

Fig. 5.4 **a** Schematic of the influence of foraminiferal physiology on the carbonate chemistry of the microenvironment. *Circles* indicate water conditions; *grey arrows* indicate DIC drawdown via photosynthesis, DIC release via respiration, and alkalinity and DIC drawdown (in a 2:1 ratio) via calcification; *black arrows* show the net influence of these processes. For simplicity, the minor alkalinity changes due to nitrate uptake and release have been ignored. While respiration and photosynthesis stay constant with changing carbonate chemistry, calcification is likely to vary as a function of saturation state, driving variable offsets in $\delta^{11}B$ of borate between the foraminiferal microenvironment and the surrounding seawater. **b**, **c** An equilibrium calculation of $\delta^{11}B$ offsets in the foraminiferal microenvironment. Note that this is a major simplification compared to the Wolf-Gladrow et al. (1999) and Zeebe et al. (2003) approach, but useful for building intuition. Bulk solution conditions have DIC of 1800 µmol/kg and alkalinity of 1800–3000 µmol/kg, giving a range of pH and $\delta^{11}B$ of borate values. The *green dashed lines* show the influence of 75 µmol/kg DIC drawdown via photosynthesis and 75 µmol/kg DIC release via respiration on $\delta^{11}B$ in the foraminiferal microenvironment. The *gray dot-dash line* shows the combined influence of calcification, which draws down alkalinity and DIC in a 2:1 ratio as a function of 2 $(\Omega - 1)^{1.9}$, and 50 µmol/kg net DIC release via respiration. Also plotted are the wild *O. universa* data of Henehan et al. (2016) and the cultured *O. universa* data of Sanyal et al. (1996), plotted as in Fig. 5.3. The *black arrow* indicates the magnitude of $\delta^{11}B$ offset in *O. universa* observed between *light* and *dark* culture conditions (Hönisch et al. 2003), and the *gray* band indicates $\Omega_{calcite}$ found in typical modern surface ocean conditions (i.e. covering the full habitat range of *O. universa* and excluding only low Ω waters from the high latitude Southern Ocean and North Pacific). Changes in calcification as a function of carbonate ion saturation may drive variable $\delta^{11}B$ offsets in the extremely wide range of saturation states created under culture conditions, whereas offsets remain constant for surface ocean values of $\Omega_{calcite}$. All plots are given for 25 °C, 35 psu and 0 m water depth, with calculations carried out in CO2SYS.m (van Heuven et al. 2009)

discussion about fractionation of boron into carbonates (for instance see supplementary information of Hönisch et al. 2009). While inorganic precipitate data might be hoped to provide constraints on inorganic equilibrium and/or kinetic fractionation, the unexplained discrepancies between different studies (discussed in Sect. 3.2.1) currently make it difficult to derive unambiguous fractionation factors from this work. Much of the discussion of boron fractionation during carbonate formation has thus been based on $\delta^{11}B$ in biogenic carbonates.

As discussed above, benthic foraminifera appear to follow $\delta^{11}B$ of borate with no significant offset (Figs. 5.2 and 5.3). However planktic foraminifera show a range of offsets (Fig. 5.3), some of which vary as a function of pH (i.e. the $\delta^{11}B$ data have a different "slope" or sensitivity to pH compared to borate). In corals, large offsets above $\delta^{11}B$ of borate are commonly attributed to internal pH elevation (Hönisch et al. 2004; Krief et al. 2010; McCulloch et al. 2012b; Allison and Finch 2010; Allison et al. 2014 and see Chap. 5 by McCulloch), but this appears not to exert major influence in most foraminifera (see further discussion below). In foraminifera, the physiological processes of photosynthesis, respiration, and calcification are well-documented to cause pH modification in the microenvironment (Rink et al. 1998; Köhler-Rink and Kühl 2000). Zeebe et al. (2003)'s reaction-diffusion model suggested that boron isotope offsets due to these processes

may stay constant across a range of pH, making the variable offsets hard to explain. However variable offsets may occur if the nature of carbonate precipitation changes over the range of culture conditions.

Variable $\delta^{11}B$ offsets may be expected to arise due to changes in the buffering capacity of the carbonate system at different pH. At low pH, a given change in DIC (for instance via photosynthesis) will drive a larger change in pH than at higher absolute pH values (Fig. 5.4a; and see Allison and Finch 2010). This appears at first to provide a possible explanation for the larger offsets from $\delta^{11}B$ of borate observed in foraminifera cultured at low pH. However the effect of this on the boron isotope system is countered by the reduced sensitivity of $\delta^{11}B$ of borate at lower pH (the flattening of the $\delta^{11}B$ of borate curve in Fig. 5.2b). Thus although the size of the pH offset resulting from a constant photosynthetic DIC-drawdown may change at different bulk solution pH, the offset in $\delta^{11}B$ remains relatively constant. This is illustrated by the schematic in Fig. 5.4a: the photosynthesis DIC-drawdown vectors cross 0.1 pH units at high pH and 0.2 at low pH, but in both cases cross ~2 permil in $\delta^{11}B$ of borate. This is also shown with simple steady state calculations in Fig. 5.4b, c: the offset between $\delta^{11}B$ of borate in the bulk solution and the green dashed lines (depicting a constant DIC-drawdown or addition) stays relatively constant with solution pH, as shown more comprehensively in Zeebe et al. (2003)'s diffusion-reaction model.

Variable $\delta^{11}B$ offsets may instead be explained by changes in physiology as a function of pH. Photosynthesis and respiration rates are not thought to be substantially impacted by changes in the carbonate system of this magnitude (Glas et al. 2012a). (Though a potential exception to this is noted by Henehan et al. (2013), who observe that cultured *G. ruber* holds its symbionts closer to its test under low pH conditions, which may increase the intensity of photosynthetic elevation of pH and $\delta^{11}B$ at low pH.) Calcification rate, on the other hand, is expected to vary substantially as a function of changes in carbonate saturation (Ω) over the range of pH values used in culture studies (e.g. Bijma et al. 2002). For instance calcite saturation state varies from ~1.5 to 20 over the pH_{tot} range of 7.6–8.9 used in Sanyal et al. (1996); a generalized calcite precipitation rate law of $R = 2(\Omega - 1)^{1.9}$, gives a factor of 1000 change in precipitation rate over this range. Carbonate precipitation draws down local pH by removing 2 mol of ALK for every 1 of DIC (Fig. 5.4a). Rapid $CaCO_3$ precipitation at high saturation states may thus drive large decreases in microenvironment pH (Glas et al. 2012b; Toyofuku et al. 2017), compared to slower $CaCO_3$ precipitation at lower saturation states giving smaller local pH decrease (Fig. 5.4a). This may act to decrease $\delta^{11}B$ values in foraminiferal carbonate in cultures at high pH and saturation state, and thus give $\delta^{11}B$ in cultured foraminifera a relatively "shallow slope" or reduced sensitivity to $\delta^{11}B$ of borate as a function of pH.

The potential influence of variable calcification rates on foraminiferal microenvironment is illustrated with the simple steady state calculation in Fig. 5.4b, c. This calculation alters the carbonate system for a modelled microenvironment compared to the bulk solution by ALK and DIC drawdown in a 2:1 ratio as a function of saturation state, along with a constant net DIC-drawdown due to net respiration. This equilibrium treatment is a (gross!) simplification of variable rates of carbonate precipitation, and it should also be noted that foraminifera may not follow this precipitation rate law (see Allen et al. 2016, though note that crystal growth rate may vary substantially from mass added in culture). However this calculation does illustrate the potential for the extremely large range of saturation states experienced in culture to cause reduced sensitivity of foraminiferal $\delta^{11}B$ to pH ("shallow slopes"), as observed in culture (Fig. 5.4b, c).

The reduced sensitivity of planktic foraminiferal $\delta^{11}B$ to pH displayed in culture is not readily observed in wild samples of planktic or benthic foraminifera (Figs. 5.3 and 5.4b, c), although it should be noted that few wild calibration studies span a large-enough pH range to precisely constrain this sensitivity. Nonetheless,

the recent wild *O. universa* data of Henehan et al. (2016) follow the pH sensitivity of $\delta^{11}B$ of borate more closely than previous *O. universa* cultures (Sanyal et al. 1996). This might be explained by the different character of carbonate system changes under culture versus natural conditions. While many culture experiments make large alkalinity changes at constant DIC, resulting in an extremely large range of carbonate saturation states ($\Omega_{calcite}$ of ~1.5–20), in natural conditions alkalinity and DIC changes are often coupled, and changes in saturation state are muted by carbonate compensation. Furthermore on long timescales, changes in ocean carbonate saturation are buffered compared to changes in pH (Tyrrell and Zeebe 2004; Hönisch et al. 2012). Therefore if the large range of carbonate saturation is the chief cause of reduced sensitivity of cultured $\delta^{11}B$ to pH, then calibration data obtained from wild samples may be more applicable to the geological record. Further work is required to test this idea and to further improve calibrations of foraminiferal $\delta^{11}B$ to pH under both culture and wild conditions.

5.3.2.3 Boron Isotope Constraints on Biomineralisation

The sensitivity of boron isotopes to pH makes them a powerful constraint on mechanisms of calcification in foraminifera. Here I briefly discuss the influence of some potential calcification processes on boron isotopes in foraminifera, and speculate on models that may match the constraints from $\delta^{11}B$. Note that as the timescale of boron isotope equilibration is extremely fast (~125 μs; Zeebe et al. 2001), kinetic processes are unlikely to exert a primary influence, simplifying interpretations compared to $\delta^{18}O$ and $\delta^{13}C$ (Zeebe and Wolf-Gladow 2001).

A common feature of many models of calcification is the elevation of pH in a somewhat isolated volume of seawater (de Nooijer et al. 2014). pH elevation of ~0.5–1 units above ambient seawater has indeed been observed during calcification in foraminifera (de Nooijer et al. 2009; Bentov et al. 2009) and corals (Venn et al. 2011) using fluorescent dyes. However while high $\delta^{11}B$ in corals appears to reflect this pH elevation (see Chap. 6 and McCulloch et al. 2012a; Krief et al. 2010; Anagnostou et al. 2012; Allison et al. 2014), $\delta^{11}B$ in most foraminifera does not: pH elevation of 1 pH unit should give $\delta^{11}B$ ~7–14‰ above seawater borate (Fig. 5.5), but most foraminifera lie within a few permil of borate ion at seawater pH (Figs. 5.3 and 5.5).

The impact of pH elevation on foraminiferal $\delta^{11}B$ may be even greater if boric acid is able to diffuse from seawater to the site of pH elevation, where it would re-equilibrate and elevate the total (or "seawater") $\delta^{11}B$ of the calcifying solution above 39.61‰. Rayleigh fractionation also has the potential to elevate $\delta^{11}B$ in an isolated volume of seawater, due to progressive drawdown of borate into carbonate, but the low partitioning of boron into calcite negates this effect (Rae et al. 2011; Stewart et al. 2016).

To date, substantial influence of pH elevation on foraminiferal $\delta^{11}B$ has only been suggested from one study, based on SIMS analyses of cultured *Amphistegina lobifera* (Rollion-Bard and Erez 2010). In these specimens the lowest $\delta^{11}B$ values from individual SIMS spots fall close to $\delta^{11}B$ of borate at ambient culture water pH, while the highest $\delta^{11}B$ values reach an upper limit of ~30‰, equivalent to a pH of ~8.9. Notably, this is similar to pK_2, the second equivalence point of carbonic acid, above which the overwhelming majority of DIC is present as CO_3^{2-}. pH elevation above this point would thus give no further increase in carbonate saturation and may also impact carbon concentration mechanisms. Whatever the causal mechanism, these data thus appear to suggest well-regulated pH elevation up to a chemically-determined limit (see also Gagnon et al. 2013 and Toyofuku et al. 2017), with calcification at pHs between this limit and ambient seawater (Rollion-Bard and Erez 2010; and see green lines in Fig. 5.5a). However in a separate study using LA-MC-ICPMS, Kaczmarek et al. (2015) find large negative $\delta^{11}B$ offsets in cultured *Amphistegina*, which are hard to reconcile with pH elevation (though one possible explanation is discussed below). The results from these high Mg foraminifera thus remain somewhat enigmatic.

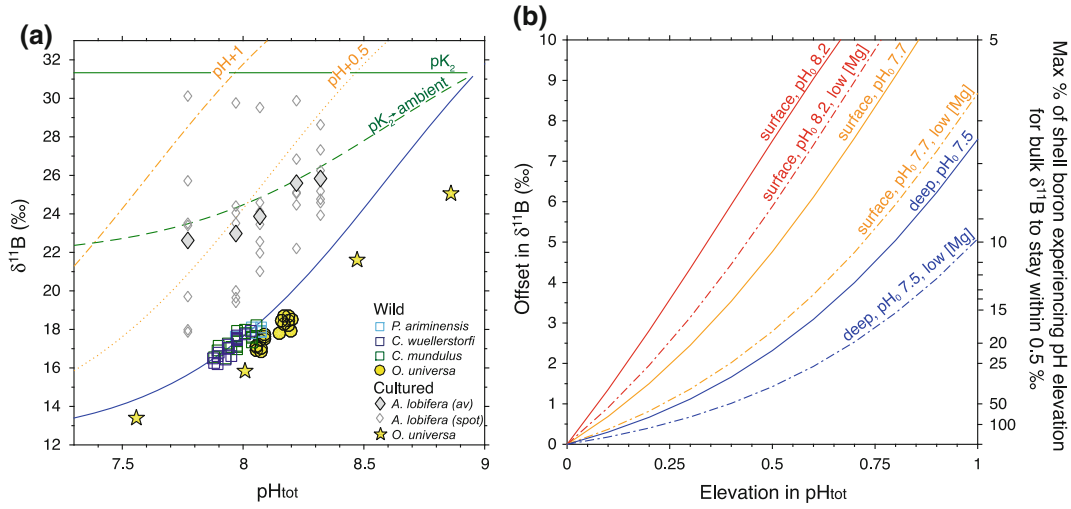

Fig. 5.5 **a** Boron isotope composition of borate ion under different pH elevation scenarios. The *blue curve* shows ambient water conditions. The *orange dotted* and *dot-dash lines* show pH elevation of 0.5 and 1.0. The *green solid line* shows pH elevation to the equivalence point of HCO_3^- and CO_3^{2-} (pK_2), and the *green dashed line* shows the mean of conditions at pK_2 and in ambient water. This illustrates a scenario where pH elevation initiates calcification, and pH then falls as calcification takes place, giving $\delta^{11}B$ offsets that fall between elevated and ambient conditions. Foraminiferal boron isotope data are also shown, including wild epifaunal benthic species (Rae et al. 2011; *open squares*), wild *O. universa* (Henehan et al. 2016; *yellow circles*), cultured *O. universa* (Sanyal et al. 1996), and cultured *A. lobifera* (Rollion-Bard and Erez 2010; open diamonds showing individual SIMS spots on a single foraminifera and filled diamonds their mean). All scenarios are calculated for surface water conditions at 25 °C, 35 psu and 0 m water depth, and foraminiferal data have been adjusted to these conditions (as described in Fig. 5.5 3 and Sect. 5.3). **b** Offset between boron isotope composition of borate under different pH elevation scenarios compared to ambient seawater conditions. *Red* and *Orange lines* show surface conditions (25 °C, 35 psu and 0 m water depth), with initial ambient water pH (pH_0) of 8.2 and 7.7. *Blue lines* show deep water conditions (0 °C, 35 psu and 2000 m water depth) with pH_0 of 7.5. *Dot-dash lines* show conditions with magnesium lowered to 3 mmol/kg (Hain et al. 2015). This is similar to the magnesium concentration predicted for the site of calcification in low-Mg foraminifera using inorganic partition coefficients. (In contrast, calcium concentration has relatively little influence on these relationships; Fig. 5.5 1d). Right hand axis shows the maximum proportion of boron that could have been incorporated into a foraminiferal shell under elevated pH, while still allowing bulk shell $\delta^{11}B$ to fall within 0.5‰ of borate at ambient seawater pH, as observed in symbiont-barren epifaunal benthic taxa

As the low-Mg benthic and planktic foraminifera have $\delta^{11}B$ values close to $\delta^{11}B$ of borate at seawater pH, the majority of the boron incorporated into these genera seems unlikely to have been derived directly from a seawater pool that experienced large pH elevation (Fig. 5.5). However this must be reconciled with the observations that at least some seawater *is* present during chamber formation (de Nooijer et al. 2009; Bentov et al. 2009; Nehrke et al. 2013) and that pH elevation *does* occur in a range of genera (de Nooijer et al. 2009; Bentov et al. 2009). Possible mechanisms that may satisfy these apparently contradictory observations include:

(1) borate that reaches the calcifying space being (selectively) removed from seawater at seawater pH;
(2) notable pH elevation occurring only during initial chamber formation, while the bulk of the shell is precipitated at a pH close to seawater, perhaps aided by Mg-removal;
(3) initial pH elevation being countered by carbon concentration and/or carbonate precipitation;
(4) pH elevation being less pronounced in the wild than during culture observations.

If borate ion is selectively transported from seawater to the calcifying space, without input of bulk seawater or boric acid, then pH could vary without impacting shell $\delta^{11}B$, provided that all of the borate in this pool is incorporated (Rae et al. 2011). Selective transport could potentially be achieved by trans-membrane ion channels, which have been proposed by some authors to deliver significant portions of calcium (Nehrke et al. 2013; de Nooijer et al. 2009; Toyofuku et al. 2008), and potentially also DIC (de Nooijer et al. 2014), to the calcifying space. It has been suggested that Ca^{2+} channels might be "leaky" to Mg^{2+}, given its similar size and charge (Raitzsch et al. 2010; de Nooijer et al. 2009); likewise it is possible that HCO_3^- transporters could be leaky to $B(OH)_4^-$. However the presence of membrane-impermeable dyes and beads at the site of calcification (Bentov and Erez 2006; Nehrke et al. 2013; de Nooijer et al. 2009) and in calcite itself (Bentov and Erez 2006) shows that bulk seawater—and not just channel-derived ions—must reach the site of calcification. Given the high concentration of boron in seawater this would likely dominate the total boron in the calcification space, so pH elevation would elevate foraminiferal $\delta^{11}B$. Selective transport of borate is thus unlikely to offer a silver bullet to explain the match between seawater borate and foraminiferal $\delta^{11}B$. However if borate transport does occur, it could potentially help counter elevation of $\delta^{11}B$ due to pH elevation, by reducing $\delta^{11}B$ of bulk boron in the calcification space.

Alternatively the lack of an obvious signal of pH elevation in low-Mg foraminifera could be explained if pH elevation only occurs during initial chamber formation, with the majority of calcification taking place at pH closer to seawater. Bulk shell $\delta^{11}B$ could be kept within 0.5‰ of seawater borate if pH elevation of 0.5 units is only experienced by ~5–25% of the boron incorporated into foraminiferal calcite (depending on environmental conditions; Fig. 5.5b). The rest of the boron could be sourced from borate ion adsorbed and incorporated during thickening of calcite onto existing chambers, if this process takes place at pH close to ambient seawater. The challenge to such a scenario is finding mechanisms to drive calcification under these conditions.

Calcification at pH close to ambient may perhaps be facilitated by active magnesium removal (Bentov and Erez 2006). Mg-removal acts to increase the activity of carbonate ions and reduce Mg "poisoning" of calcite growth (Zeebe and Sanyal 2002), and has been suggested to occur via mitochondrial activity in pseudopods surrounding the shell (Spero et al. 2015). Mg-removal has particular relevance to boron isotopes because reduced Mg concentrations notably increase K_B (Fig. 5.1d), reducing the sensitivity of $\delta^{11}B$ to changes in pH (Fig. 5.5b). For instance reducing Mg concentrations at the site of calcification to ~3 mol/kg (as predicted using inorganic partition coefficients and Mg concentrations in low-Mg foraminifera) may reduce the impact of 0.5 units pH elevation on $\delta^{11}B$ from ~5 to ~3‰ depending on initial conditions (Fig. 5.5b). Mg-removal would also reduce the impact of local pH decrease during calcification (see below). Different degrees of Mg removal from the calcifying space may also partially explain the contrasting $\delta^{11}B$ offsets between taxa with different Mg/Ca (Fig. 5.5): extensive Mg-removal in low-Mg benthic and planktic species would minimise the impact of local pH changes on $\delta^{11}B$; in contrast minimal Mg-removal in high-Mg taxa such as *Amphistegina* renders their boron isotope composition highly sensitive to pH changes during biomineralisation.

The influence of pH elevation during initial chamber formation on $\delta^{11}B$ may also be countered by local reductions in pH due to DIC concentration or during calcification. Bentov et al. (2009) demonstrate the presence of low-pH vacuoles during calcification, which they suggest may drive carbon concentration via CO_2 diffusion to low-CO_2/high-pH seawater vacuoles (see Allison et al. 2014 for analogous process in corals). Indeed were CO_2 diffusion infinitely efficient, DIC addition would keep pace with pH elevation, resulting in minimal net elevation in pH or $\delta^{11}B$. The fact that high pH vacuoles are observed demonstrates that DIC addition is not as efficient as in this end member scenario.

Nonetheless, concentration of CO_2 seems likely to play a role in minimizing offsets in $\delta^{11}B$.

Acidification of the calcifying microenvironment may also occur due to net alkalinity drawdown during calcification (Fig. 5.4a), and indeed could act as a negative feedback on calcification. To combat this, foraminifera have been shown to actively extrude H + from the calcifying space into surrounding seawater (Glas et al. 2012b), using a V-ATPase "proton-pump" (Toyofuku et al. 2017). Nonetheless, depending on the efficiency of this pump, some degree of acidification at the site of calcification may still occur. Acidification of the seawater surrounding the foraminifera is also likely to drive further CO_2 diffusion to the site of calcification, increasing DIC and countering some of the initial pH elevation (Toyofuku et al. 2017). Furthermore, if this low-pH water is vacuolised and transported to the site of calcification, it could not only counter the influence of initial pH elevation, but may even produce negative offsets between foraminiferal $\delta^{11}B$ and seawater borate (Fig. 5.4). The magnitude of these influences will be highly dependent on calcification rate and diffusion in the shell's microenvironment, which may differ between settings, and could perhaps provide a mechanism to explain differences in *Amphistegina* $\delta^{11}B$ between studies (Rollion-Bard and Erez 2010; Kaczmarek et al. 2015).

Finally it is possible that active pH manipulation may be most pronounced under the warm and energy-rich conditions in lab cultures, and less pronounced in the wild, in particular in cold deep-sea environments with low food. The reduced sensitivity of $\delta^{11}B$ to pH in cold, low-pH environments (Fig. 5.5b) may also contribute to the absence of a pH elevation signal in wild *Cibicidoides* from the deep ocean, despite the fact that pH elevation has been observed in this genera under culture conditions (de Nooijer et al. 2009). Higher turbulence in the wild may also help minimize pH gradients in the microenvironments surrounding calcifying foraminifera (Glas et al. 2012b; Toyofuku et al. 2017).

In summary, the close correspondence between $\delta^{11}B$ of foraminifera and seawater borate provides useful constraints on pH during calcification. Trans-membrane transport of borate ion is unlikely to explain this signal (in contrast to the suggestion of Rae et al. 2011), as it will be overwhelmed by boron from the seawater that is present at the site of calcification. DIC concentration and acidification during calcification could in part counter pH elevation; however at least some of this acidification is a result of actively extruded protons, which will maintain elevated pH at the site of chamber formation. Furthermore although scenarios that balance extremely high and low pH influences are possible, it seems unlikely that they could consistently produce small $\delta^{11}B$ offsets if they account for the majority of the shell's boron. One possible scenario is that the majority of the shell's boron is incorporated at pH close to seawater during chamber thickening, with pH elevation only employed during initial chamber formation and partially offset by concentration of DIC. Magnesium removal may help drive this secondary thickening, and would also reduce the sensitivity of $\delta^{11}B$ to further change in pH. Indeed variable Mg-removal, along with environmental influences on pH-$\delta^{11}B$ sensitivity, foraminiferal energy budgets, and variable efficiency of DIC concentration, may contribute to variable $\delta^{11}B$ offsets between taxa. Further observations are required to test this model, including better estimates of the mass balance of calcite and boron from primary chamber formation versus secondary thickening (Allen et al. 2011; Raitzsch et al. 2011). Nonetheless, it is interesting to consider that pH elevation may only be used to promote rapid initial chamber formation, with foraminifera expending energy to quickly overcome the thermodynamic barriers and physiological vulnerabilities of this process, whereas the bulk of the shell—and its boron—may be precipitated onto an existing calcite template at pH closer to seawater.

5.4 $\delta^{11}B$-Derived pH and CO_2

Interest in the boron isotope composition of foraminifera stems largely from its application as a tracer of the CO_2 system in the geological

past (Fig. 5.6). Below I describe the processes and assumptions that allow foraminiferal $\delta^{11}B$ to be converted to pH and CO_2. However it should be noted that even without further conversion, $\delta^{11}B$ of borate, as tracked by foraminiferal $\delta^{11}B$, provides a powerful tracer of carbonate system changes in its own right. Indeed, over much of the ALK-DIC space in the modern ocean, $\delta^{11}B$ of borate is a more linear tracer of ALK/DIC ratio—and $[CO_3^{2-}]$ and pCO_2—than is pH (see inset figure in Box 1). Thus provided timescales are short enough that $\delta^{11}B_{sw}$ can be assumed to have remained relatively constant (<10 Myr; see below), foraminiferal $\delta^{11}B$ alone provides a valuable tracer of relative changes in past CO_2 system conditions, and plotting raw $\delta^{11}B$ data is a valuable first step in any record. Indeed this is somewhat analogous to foraminiferal $\delta^{18}O$, which reflects both temperature and $\delta^{18}O_{sw}$, but is typically provided with no further conversion, and provides a valuable tracer of past oceanographic conditions in this raw form. Furthermore, it should be noted that despite uncertainties in absolute pH and CO_2 values arising from estimates of $\delta^{11}B_{sw}$ and a second carbonate system parameter, relative changes in pH and CO_2 may still be well constrained. Indeed Foster and Rae (2016) demonstrate that estimates of climate sensitivity in the past, based on comparison of $\delta^{11}B$-derived CO_2 to sea surface temperature, are relatively insensitive to uncertainties in $\delta^{11}B_{sw}$ and estimates of alkalinity.

5.4.1 pH from $\delta^{11}B$

5.4.1.1 $\delta^{11}B$ of Borate and pH

The first step in obtaining pH from foraminiferal $\delta^{11}B$ is conversion to $\delta^{11}B$ of borate. This is achieved using the calibrations described above and shown in Fig. 5.3 (see also Foster and Rae 2016). Ideally the calibration used would be based on foraminifera collected under wild conditions, as these should most accurately reflect the combination of influences felt by open ocean foraminifera taken from samples "down-core". However in many cases these wild calibrations do not span a wide range of pH and so culture calibrations are also commonly applied. As discussed above, some culture calibrations have lower sensitivity to $\delta^{11}B$ borate changes than wild calibrations, and more work is required to determine which is most appropriate for the geological record. Careful micropalaeontoloty is also required to assess the most appropriate calibrations to use for extinct species (Anagnostou et al. 2016).

With $\delta^{11}B$ of borate determined, conversion to pH is typically achieved using Eq. (5.9), which is based on the approximation provided by Eq. (5.6).

$$pH = pK_B - \log\left(-\frac{\delta^{11}B_{SW} - \delta^{11}B_{B(OH)_4^-}}{\delta^{11}B_{SW} - \alpha_B.\delta^{11}B_{B(OH)_4^-} - \varepsilon_B}\right) \quad (5.9)$$

More accurately, using Eqs. (5.2) and (5.7), we obtain the expression in Eq. (5.10) below.
Conversion of $\delta^{11}B$ borate to pH thus requires knowledge of K_B and $\delta^{11}B_{sw}$.

$$pH = -\log_{10}\frac{K_B \cdot {}^{\frac{11}{10}}R_{B(OH)_4^-} - K_B \cdot {}^{\frac{11}{10}}R_{SW} + \alpha_B \cdot K_B \cdot {}^{\frac{11}{10}}R^2_{B(OH)_4^-} - \alpha_B \cdot K_B \cdot {}^{\frac{11}{10}}R_{SW} \cdot {}^{\frac{11}{10}}R_{B(OH)_4^-}}{{}^{\frac{11}{10}}R_{SW} + {}^{\frac{11}{10}}R_{SW} \cdot {}^{\frac{11}{10}}R_{B(OH)_4^-} - \alpha_B \cdot {}^{\frac{11}{10}}R_{B(OH)_4^-} - \alpha_B \cdot {}^{\frac{11}{10}}R_{B(OH)_4^-}} \quad (5.10)$$

5.4.1.2 K_B

The equilibrium constant of boric acid, K_B, is a well-defined function of temperature, salinity, and pressure, given by the expression (Dickson 1990):

$$\begin{aligned} K_B = \exp[((&- 8966.9 - 2890.53 * S^{1/2} \\ &- 77.942 * S + 1.728 * S^{3/2} - 0.0996 * S^2))/Tk \\ &+ 148.0248 + 137.1942 * S^{1/2} + 1.62142 * S \\ &+ (-24.4344 - 25.085 * S^{1/2} - 0.2474 * S) * \ln(Tk) \\ &+ 0.053105 * S^{1/2} * \ Tk] \end{aligned} \tag{5.11}$$

with the formula below giving the correction for different pressures:

$$\begin{aligned} P_{factor} = &(29.48 - 0.1622 * Tc \\ &+ 0.002608 * Tc^2)/(R*Tk) * P... \\ &+ 0.5 * (-0.00284)/(R*Tk) * P^2 \end{aligned} \tag{5.12}$$

$$K_B = \exp\ (\ln K_B\ +\ P_{factor}) \tag{5.13}$$

where S is salinity, Tk is temperature in Kelvin, Tc is temperature in Celcius, P is pressure in bars (equivalent to depth in meters divided by 10), and R is the gas constant (83.14472 cm^3 bar K^{-1} mol^{-1}; Dickson et al. 2007). Note that the influence of these environmental parameters on the conversion of $\delta^{11}B$ of borate to pH is relatively minor over the conditions likely to be found at a given site: changes of ±5 °C, ±1 psu, and ±100 m result in differences in $\delta^{11}B$ borate of ~0.35‰, 0.05‰, and 0.03‰ respectively, for $\delta^{11}B$ borate of ~15‰ at 25 °C, 35 psu and 100 m water depth (Fig. 5.1c). Matlab codes and an Excel spreadsheet that carry out these calculations are provided in the supplementary online materials.

The composition of seawater can also influence K_B, in particular due to ion pairing of Ca and Mg ions with borate (Hershey et al. 1986; Nir et al. 2015; Hain et al. 2015). Hain et al. (2015)'s MyAMI ion pairing model shows that pK_B is relatively insensitive to the changes in [Ca] seen over the Cenozoic, though more sensitive to [Mg] (Fig. 5.1d). For instance $\delta^{11}B$ of borate of 16‰, at 25 °C, 35 psu, 0 m water depth, and with modern $\delta^{11}B_{sw}$, yields pH of 7.82 under modern [Ca] of 10 M and [Mg] of 52 M, 7.84 under Miocene [Ca] of 14 M and [Mg] of 48 M, and 7.94 under Eocene [Ca] of 20 M and [Mg] of 30 M (Horita et al. 2002; Hain et al. 2015). Note that equivalent calculations using the Pitzer ion pairing model available with PHREEQ give slightly larger changes in pK_B (Nir et al. 2015).

5.4.1.3 $\delta^{11}B$ of Seawater

The boron isotope composition of modern seawater is 39.61 ± 0.04‰ (Foster et al. 2010). Boron has a long residence time in seawater of ~10 Myr, and modelling suggests that typical rates of change for $\delta^{11}B_{sw}$ over the last ~100 Myr are of the order 0.1‰/Myr (Lemarchand et al. 2000). $\delta^{11}B_{sw}$ may thus be assumed to have remained within analytical error of modern values for the last ~3 Myr, and $\delta^{11}B$ records spanning a few million years should be dominantly a function of change in pH rather than $\delta^{11}B_{sw}$. However for accurate reconstruction of absolute pH values beyond ~3 Ma and for interpretation of $\delta^{11}B$ records spanning multiple millions of years, constraints on past $\delta^{11}B_{sw}$ are required (see Figs. 5.6 and 5.8).

Three general approaches have been used to reconstruct $\delta^{11}B_{sw}$:

(1) box modelling, using estimates of oceanic input and output fluxes over time;
(2) measurement of substances, such as pore waters and halites, with $\delta^{11}B$ close to that of ancient seawater;
(3) measurement of carbonate $\delta^{11}B$ where independent constraints can be placed on pH.

Box models of $\delta^{11}B_{sw}$ must take account of source terms, including weathering flux in rivers (Lemarchand et al. 2000), hydrothermal venting (Smith et al. 1995), and fluids from accretionary prisms (You et al. 1993), and sink terms, including oceanic crust alteration (Spivack and Edmond 1987), adsorption onto clays (Spivack et al. 1987), and incorporation in carbonates (Hemming and Hanson 1992). These terms are not well

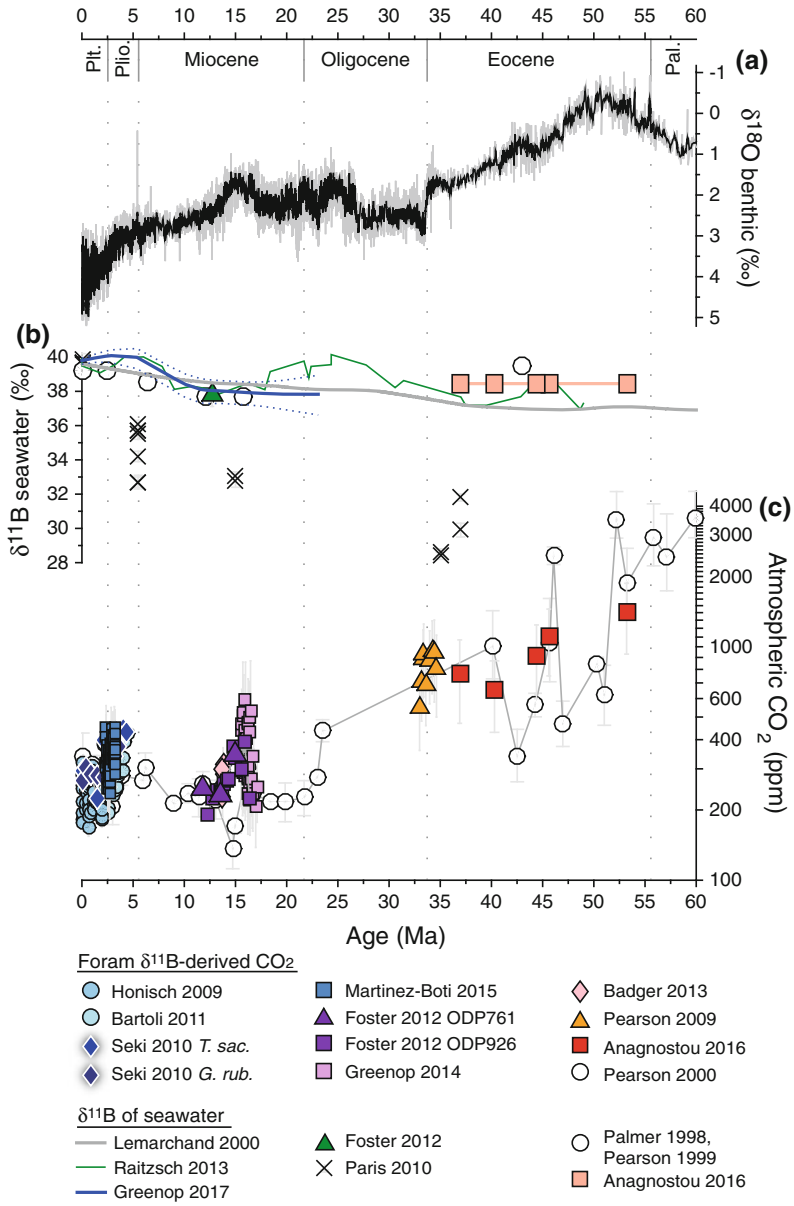

Fig. 5.6 Compilation of δ^{11}B-based CO_2 reconstructions and $\delta^{11}B_{SW}$ estimates for the Cenozoic. **a** Benthic $\delta^{18}O$ compilation (Zachos et al. 2001, 2008; *grey line*) with a 5 point moving average (*black line*). Heavier values indicate cooler temperatures and greater continental ice volume (note reverse scale). **b** Estimates of $\delta^{11}B$ of seawater. Halite data lighter than 28‰ are not plotted; note that Paris et al. (2010b) also suggest that several of the lightest halite values in the intervals shown may be excluded. The Lemarchand et al. (2000) model output is shown for the scenario of constant riverine input. The Greenop et al. (2017) curve is shown with its 2σ error envelope. The Raitzsch and Hönisch (2013) estimate is their scenario using alpha from Klochko et al. (2006) and assuming a linear change in pH over the Cenozoic. **c** pCO_2 reconstructions based on foraminiferal $\delta^{11}B$. Where different estimates of $\delta^{11}B_{SW}$ or second carbonate system parameters were given, the assumptions favored in the original publication are shown. Note the long term decrease in atmospheric CO_2 as climate cools over the Cenozoic and the correspondence between more rapid atmospheric CO_2 change and major climate transitions

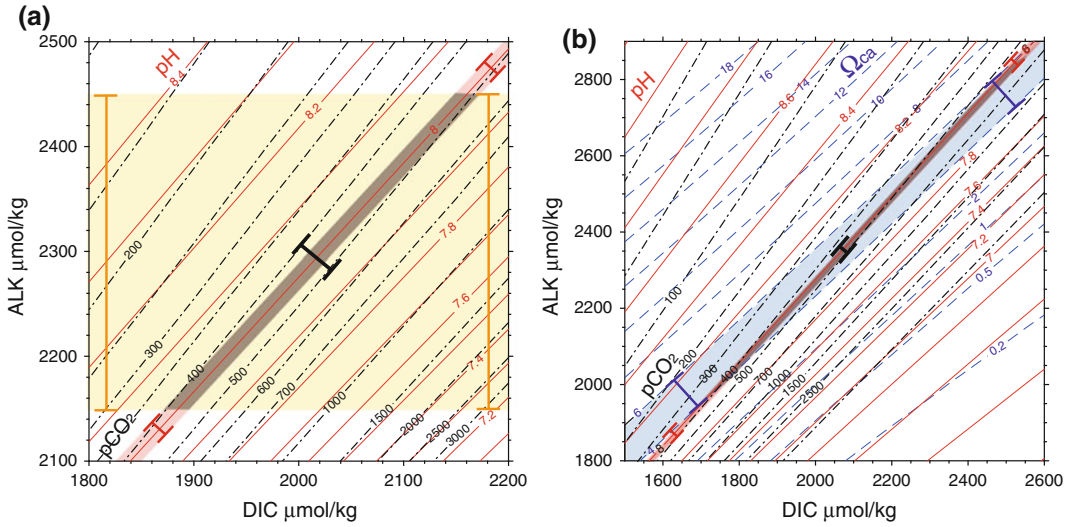

Fig. 5.7 Determination of pCO_2 from $\delta^{11}B$-derived pH, using an assumption of surface ocean alkalinity (**a**) or calcite saturation (**b**). The *red shaded* area indicates $\delta^{11}B$-derived pH of 8.0 ± 0.02; the *yellow area* in (**a**) shows alkalinity of 2300 ± 150 µmol/kg (close to the whole range in the modern surface ocean); the *light blue shaded* area in (**b**) shows $\Omega_{calcite}$ of 4–6 (thought to reflect the long-term range in the surface ocean). Overlap between the pH and second carbonate system parameter fields (*dark gray area*) constrains the range of pCO_2 values (*black error bar*). Note the close relationship between pH and pCO_2, which allows a precise determination of pH, combined with conservative estimates of alkalinity or $\Omega_{calcite}$, to still give relatively tight constraints on pCO_2. As contours of $\Omega_{calcite}$ are relatively closely aligned with pH, the use of $\Omega_{calcite}$-derived $[CO_3^{2-}]$ (**b**) provides a less precise constraint on pCO_2 than does alkalinity (**a**). All plots are given for 25 °C, 35 psu and 0 m water depth, with calculations carried out in CO2SYS.m (van Heuven et al. 2009). The scale of (**b**) is expanded compared to (**a**)

constrained over geological time, but may be proxied by more general geological processes, such as seafloor spreading rates (Simon et al. 2006) and total carbonate deposition (Lemarchand et al. 2000). Despite the uncertainties in how each of these fluxes has changed, this approach may be valuable when paired with constraints on the secular evolution of seawater chemistry from other isotopic systems (e.g. $^{87}Sr/^{86}Sr$, δ^7Li).

Measurement of archives with $\delta^{11}B$ close to ancient seawater is appealing, but it is hard to find settings where these signatures are pristine. Paris et al. (2010b) use $\delta^{11}B$ measurements on halites in evaporite deposits to reconstruct $\delta^{11}B_{sw}$ at 3 intervals over the last 40 Myr (Fig. 5.6b). This approach takes advantage of the fact that halites are one of the only solid materials with $\delta^{11}B$ similar to seawater rather than borate ion, likely due to the trapping of brine inclusions of fluid inclusions during halite growth. However $\delta^{11}B_{sw}$ determined by this method lies ~3–6‰ below other estimates, and it is possible that evaporite $\delta^{11}B$ may be influenced by fractionation during evaporation or incorporation into halite (Vengosh et al. 1992) or by riverine input in the partially isolated conditions of evaporite formation. Spivack et al (1993) used pore fluid $\delta^{11}B$ data from a carbonate-rich ODP core to estimate changes in $\delta^{11}B_{sw}$. However given the notable changes in $\delta^{11}B_{sw}$ seen in even the top few cm of pore fluids (Rae et al. 2011), use of this approach requires careful constraints on boron desorption from clays and dissolution of carbonates. Some deep pore fluids have also been shown to have quite exotic boron isotope compositions (Brumsack and Zuleger 1992), which further complicates this approach.

If pH can be independently constrained, then measurements of $\delta^{11}B$ in carbonates can be used to estimate $\delta^{11}B_{sw}$. Raitzsch and Hönisch (2013)

assume a linear increase in deep ocean pH over the last 50 Myr, and combined this with $\delta^{11}B$ measurements of benthic foraminifera to estimate $\delta^{11}B_{sw}$ (Fig. 5.6). However, it is unlikely that pH change has been linear through time, as evidenced by the unrealistically rapid changes in $\delta^{11}B_{sw}$; in this record, given boron's ~10 Myr residence time. Furthermore, use of this $\delta^{11}B_{sw}$ record with benthic $\delta^{11}B$ data would only ever reproduce the original assumption of linear change in pH.

An alternative approach instead uses measurements of carbonate $\delta^{11}B$ across an assumed or estimated pH gradient. This takes advantage of the curved relationship between $\delta^{11}B$ of borate and pH, which means that for a given change in pH, a measured $\delta^{11}B$ difference will be a function of $\delta^{11}B_{sw}$. This approach was first proposed by Palmer et al. (1998), who assumed that the pH gradient between surface and thermocline-dwelling planktic foraminifera has remained constant, and made $\delta^{11}B$ measurements on a suite of these species over the Cenozoic. Pagani et al. (2005a) point out the influence of uncertainty in habitat depth on this calculation. However Anagnostou et al. (2016) have recently shown the power of this method to give bounds on possible changes in $\delta^{11}B_{sw}$, when supported by measurements of $\delta^{18}O$ and $\delta^{13}C$, and underpinned by conservative assumptions with fully propagated uncertainties. Foster et al. (2012) and Greenop et al. (2017) have also proposed a variant of this approach based on comparison of planktic and benthic $\delta^{11}B$ measurements, with the pH gradient between them constrained by measurements of $\delta^{13}C$.

Thus while accurate determination of $\delta^{11}B_{sw}$ remains a challenge for $\delta^{11}B$-based reconstructions of the carbonate system, progress is being made—and should continue—on a number of fronts.

5.4.2 CO_2 from pH

While records of pH may be used to study the history and impact of ocean acidification, much of the interest in foraminiferal boron isotope records stems from the ability of a paleo-pH meter to reconstruct CO_2. pH and aqueous CO_2 concentrations are closely coupled in seawater, both being governed by the primary carbonate system variables alkalinity and dissolved inorganic carbon (Box 1 and Fig. 5.7). From knowledge of aqueous $[CO_2]$, along with estimates of temperature and salinity, Henry's law allows calculation of the partial pressure of atmospheric CO_2 in equilibrium with this water. Measurement of $\delta^{11}B$ in planktic foraminifera may thus be used to reconstruct atmospheric CO_2 in regions such as subtropical gyres (e.g. Figs. 5.6, 5.8 and 5.9), where oceanic and atmospheric CO_2 are close to equilibrium, or constrain the strength of CO_2 sources and sinks at high latitudes or in upwelling regions (Fig. 5.10).

The ocean carbonate system is most simply described by the 6 components alkalinity, DIC, CO_2, HCO_3^-, CO_3^{2-}, and pH, which are linked by 4 independent equations; the carbonate system thus has two degrees of freedom, so knowledge of two components allows the system to be completely determined (Box 1 and Fig. 5.7). The next most important acid-base system in seawater after CO_2 is boron, which adds 3 extra components $\left(B_{SW},\ B(OH)_3,\ \text{and}\ B(OH)_4^-\right)$ and 2 independent equations. Thus with knowledge of B_{SW}, the system continues to have 2 degrees of freedom. Complete determination of the carbonate system from $\delta^{11}B$-derived pH therefore requires a second carbonate system parameter to be known.

In any determination of the carbonate system it is crucially important to consider the relationships—and associated error propagation—between different carbonate system components (Fig. 5.7). For instance due to the sub-parallel relationship between pH and $[CO_3^{2-}]$ in ALK-DIC space, the use of these parameters to determine a less closely-related component of the system (such as DIC) results in large propagated uncertainties. Rae et al. (2011) show that even with errors of only ~0.03 in pH from $\delta^{11}B$ and ~10 μmol/kg in $[CO_3^{2-}]$ from benthic B/Ca, propagated uncertainty on DIC is ~300 μmol/kg, so although the DIC

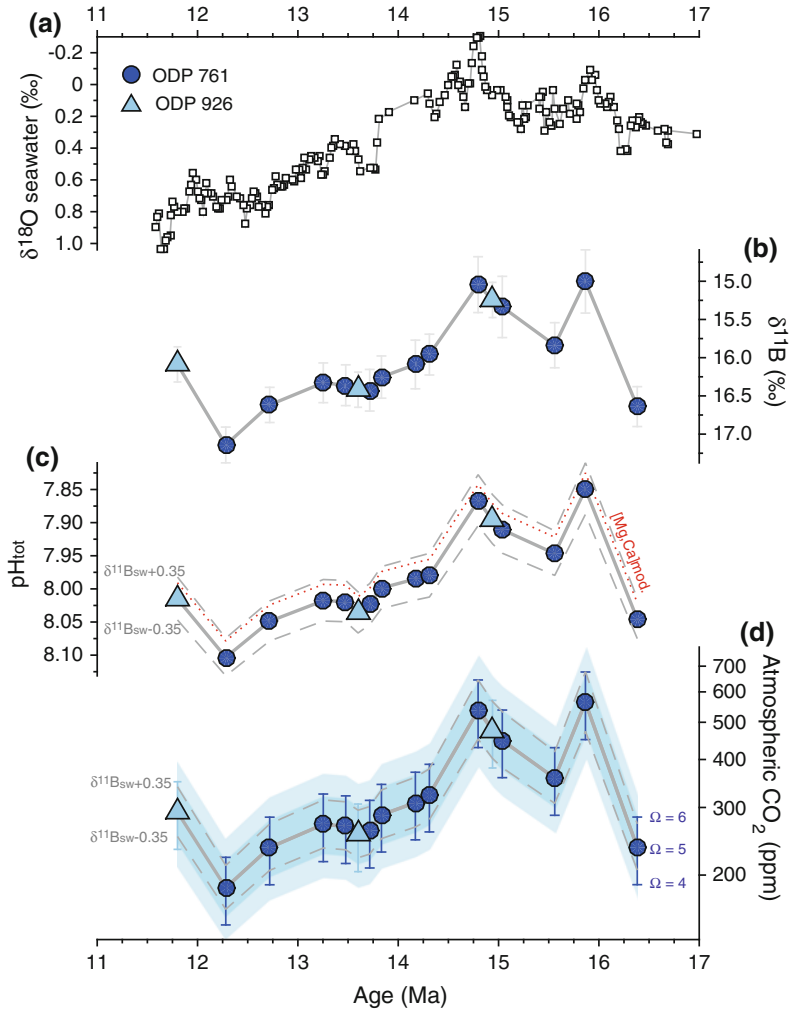

Fig. 5.8 Estimates of Miocene pH and atmospheric CO_2 from foraminiferal $\delta^{11}B$ for the Miocene, illustrating the influence of different $\delta^{11}B_{SW}$ and $\Omega_{calcite}$ values. **a** $\delta^{18}O_{SW}$ from benthic foraminiferal $\delta^{18}O$ and Mg/Ca (Lear et al. 2010), reflecting changes in global ice volume. **b** $\delta^{11}B$ of the planktic foraminifera *T. sacculifer* (formerly known as *G. sacculifer* and also known as *G. trilobus* in the Miocene; Spezzaferri et al. 2015) from ODP761 (*circles*) and ODP926 (*triangles*); (Foster et al. 2012). **c** pH calculated from $\delta^{11}B$ using the *T. sacculifer* calibration of Sanyal et al. (2001), as adjusted by Foster et al. (2012), $\delta^{11}B_{SW}$ of 37.82‰ (Foster et al. 2012), temperatures derived from Mg/Ca on these samples, and Miocene [Ca] = 14 mmol/kg and [Mg] of 48 mmol/kg (Horita et al. 2002; Hain et al. 2015). The influence of changing $\delta^{11}B_{SW}$ by ±0.35‰ (Foster et al. 2012; *grey dashed lines*) and of using modern [Ca] and [Mg] (*red dotted line*) is also shown. **d** Atmospheric CO_2 derived from the pH values in (**c**) and assuming $\Omega_{calcite} = 5 \pm 1$ (*error bars* on each point). The influence of changing $\delta^{11}B_{SW}$ by ±0.35‰ (Foster et al. 2012; *grey dashed lines*) is also shown. Confidence intervals on CO_2 of 68% and 95% (*blue shaded bands*) are derived from 1000 Monte Carlo simulations taking into account errors of ±0.2‰ on $\delta^{11}B$ measurements, ±1 °C on SST, ±1 psu on salinity, 2 mmol/kg on [Ca] and [Mg], and ±1 on $\Omega_{calcite}$. These errors are quoted at ~95% confidence and are assumed to have a normal distribution, except for $\Omega_{calcite}$ where a uniform distribution is used. Note that even without any calculation of pH or pCO_2, the close correspondence between $\delta^{11}B$ measurements and $\delta^{18}O_{SW}$ implies that CO_2 and climate are closely coupled during this interval. CO_2 calculations were carried out with a modified version of csys.m from Zeebe and Wolf-Gladow (2001). Code that reproduces this figure is available in the online materials accompanying this article

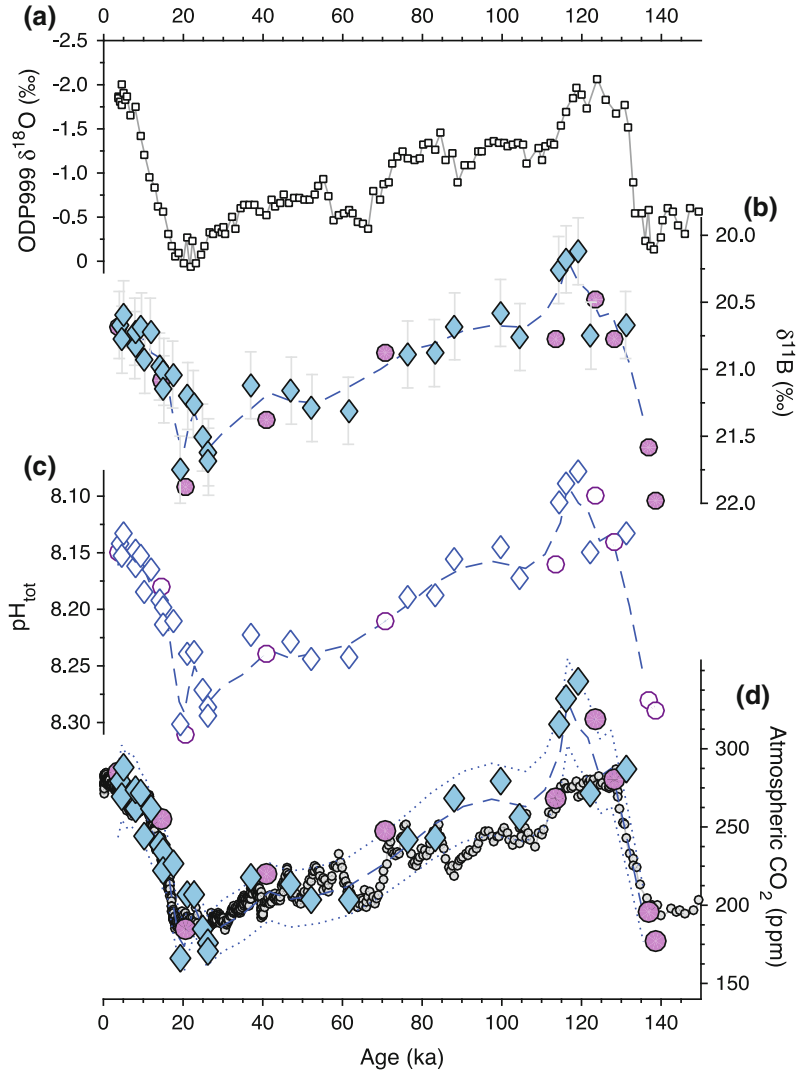

Fig. 5.9 Estimates of pH and atmospheric CO_2 for the last glacial cycle derived from foraminiferal boron isotopes. **a** $\delta^{18}O$ of *G. ruber* from ODP999 (Schmidt et al. 2004; Schmidt et al. 2006). **b** $\delta^{11}B$ of *G. ruber* from ODP999 (Foster 2008; *diamonds*) and $\delta^{11}B$ of *T. sacculifer* from ODP668 (Hönisch and Hemming 2005; *circles*). *T. sacculifer* values have been corrected to account for analytical offsets in early NTIMS measurements (see Hönisch et al. 2009), using the offset between *T. sacculifer* and *G. ruber* in these records in samples <5 kyr. The *blue dashed line* shows a 3-point moving average through the combined data. **c** $\delta^{11}B$-derived pH (*open symbols*), using the *G. ruber* calibration of Henehan et al. (2013), corrected for size fraction as in Martínez-Botí et al. (2015a), and the *T. sacculifer* calibration of Sanyal et al. (2001). **d** $\delta^{11}B$-dervied atmospheric CO_2 compared to the composite ice core record (Bereiter et al. 2015). *T. sacculifer*-derived estimates are as in the original publication (Hönisch and Hemming 2005). *G. ruber*-derived estimates are recalculated using modern alkalinity of 2330 µmol/kg and SST from Mg/Ca on the same samples (Foster 2008), and account for a modern offset of 21 ppm CO_2 between the surface ocean and atmosphere at this core site (Henehan et al. 2013). The dashed line shows a 3-point moving average through the combined data, with the *dotted lines* showing the influence of ±175 µmol/kg alkalinity (close to the whole range of the modern surface ocean)

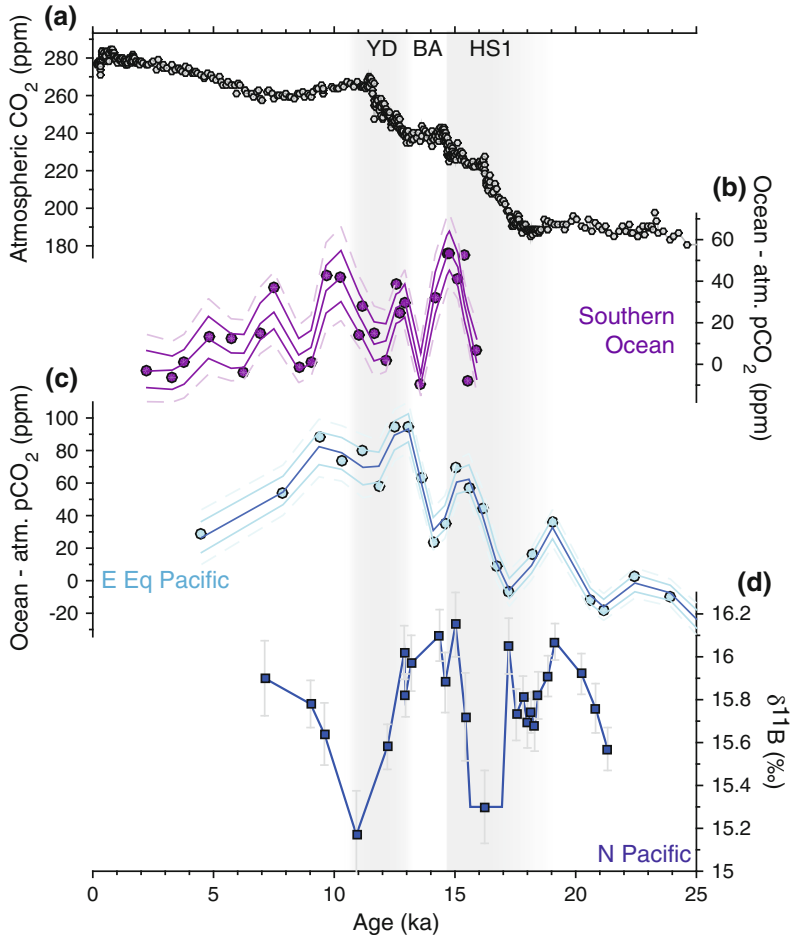

Fig. 5.10 Boron isotope records, that constrain CO_2 release from upwelling regions and the deep ocean over the last deglaciation. **a** Atmospheric CO_2 from Antarctic ice cores (Bereiter et al. 2015). **b** Ocean-atmosphere pCO_2 difference, derived from $\delta^{11}B$ on *G. bulloides* from Southern Ocean sediment core PS2498 and assuming modern alkalinity ±125 μmol/kg (Martínez-Botí et al. 2015b). *Lines* show the 68 and 95% confidence intervals calculated from 10,000 Monte Carlo simulations. **c** As in (**b**) but with $\delta^{11}B$ data from *T. sacculifer* from sediment core ODP1238 from the East Equatorial Pacific (Martínez-Botí et al. 2015b). **d** Boron isotope data from *C. wuellerstorfi* from the deep North Pacific, with error bars equivalent to 2SD on replicate measurements (Rae et al. 2014). Note the pulses of high surface water CO_2 and low deep water pH during intervals of atmospheric CO_2 rise

determination is accurate, the uncertainty spans a larger range than the whole modern ocean! However these carbonate system relationships also present opportunities, particularly in the determination of CO_2 from pH. As pH and CO_2 are very closely coupled, a well-constrained pH value will largely control the calculated CO_2 (Fig. 5.7). Therefore a reasonable estimate of a second carbonate system parameter, with generous error bars, should still result in a relatively accurate and precise determination of CO_2. Indeed it is far preferable to estimate a second carbonate system parameter with low precision that is likely to encompass the right value, than to use an estimate that is precise but inaccurate: provided the pH determination is accurate, the former approach will yield the correct CO_2 within error, while the latter will produce spurious results with the impression of high precision.

The two most commonly used second carbonate system parameters in $\delta^{11}B$-based CO_2 reconstructions are alkalinity and Ω-derived $[CO_3^{2-}]$. Alkalinity estimates in early studies (Hönisch and Hemming 2005; Foster 2008) were based on the close relationship between alkalinity and salinity in modern surface seawater: reconstructions of salinity, either from paired $\delta^{18}O$ and Mg/Ca measurements or from scaling with global sea level change, were thus used to estimate alkalinity. However alkalinity may vary independently of salinity due to changes in $CaCO_3$ cycling (Broecker and Peng 1987). Recent studies have thus used modern alkalinity but with a large range (e.g. ±175 µmol/kg; Martínez-Botí et al. 2015a) and a uniform rather than normal distribution. CO_2 is then determined via Monte-Carlo simulations, and the resulting CO_2 estimates include every possible alkalinity within the given range with equal likelihood.

On timescales beyond the last ~3 Myr the assumption that alkalinity has remained close to modern values is unlikely to hold. On these timescales several studies have used assumptions or models of calcite saturation state (Ω_{ca})

$$\Omega_{ca} = \frac{[Ca]\left[CO_3^{2-}\right]}{K_{spc}} \tag{5.13}$$

to estimate $[CO_3^{2-}]$ (Pearson et al. 2009; Anagnostou et al. 2016). It is thought that carbonate compensation maintains the global mean surface Ω_{ca} in the range 4–6 on long timescales (Ridgwell 2005; Hönisch et al. 2012; Hain et al. 2015), so given estimates of [Ca] (Horita et al. 2002) and K_{sp} (from temperature and major ion composition; Hain et al. 2015), $[CO_3^{2-}]$ can be estimated.

The ultimate test of any proxy-based reconstruction of atmospheric CO_2 is comparison to the ice core CO_2 record. This is illustrated in Fig. 5.9, demonstrating that despite the various potential sources of uncertainty, foraminiferal boron isotopes are able to provide accurate CO_2 reconstruction, with fully propagated uncertainty of ~20 ppm (2SD). Although application further back in the geological may present other challenges, the close match to ice core CO_2 demonstrates the potential of foraminiferal $\delta^{11}B$ for pH and CO_2 reconstruction.

5.5 Proxy Application: Examples

Spurred on by the development work described above, application of boron isotopes in foraminifera to the geological record has grown rapidly in recent years. Here I give a brief overview of some highlights from this work.

5.5.1 Glacial-Interglacial CO_2

Over the glacial cycles of the last 800 kyr, atmospheric CO_2 levels are well known, but the cause of CO_2 change between glacial and interglacial periods remains a mystery (EPICA 2004; Kohfeld and Ridgwell 2009). All leading hypotheses invoke changes in CO_2 partitioning between the deep ocean and the atmosphere, likely mediated by changes in circulation and productivity at high latitudes where deep waters are ventilated (Sigman et al. 2010). Boron isotope records can be used to test these hypotheses, by constraining CO_2 (dis)equilibrium between the surface ocean and the atmosphere, and CO_2 storage and release in deep waters.

A notable first application of $\delta^{11}B$ over glacial cycles was provided by Sanyal et al. (1995), who used planktic foraminifera and mixed benthic foraminifera to suggest that the pH of the ocean was ~0.3 units higher during the last glacial maximum compared to the Holocene. This was taken as support for glacial CO_2 drawdown by elevated ocean alkalinity (e.g. Archer and Maier-Reimer 1994). However reconciling this with changes in $CaCO_3$ preservation in the deep ocean is problematic (Sigman et al. 1998), and more recent work from monospecific benthics suggests much smaller changes in pH in the deep glacial ocean (Hönisch et al. 2008; Yu et al. 2010; Rae et al. 2014).

Several studies have used $\delta^{11}B$ in planktic foraminifera to reconstruct the extent of disequilibrium (ΔpCO_2) between CO_2 in surface waters and the atmosphere (Sanyal et al. 1997; Sanyal and Bijma 1999; Palmer and Pearson 2003; Foster and Sexton 2014; Naik et al. 2015; Martínez-Botí et al. 2015b; see Fig. 5.10). Recent work shows a pronounced increase in CO_2 outgassing in the East Equatorial Atlantic during the LGM (Foster and Sexton 2014), indicative of enhanced upwelling, while surface water CO_2 in the West Equatorial Atlantic stays close to equilibrium with the atmosphere, suggesting that the upwelled CO_2 and nutrients from the East are progressively drawn-down by biological productivity. In the East (Martínez-Botí et al. 2015b) and West (Palmer and Pearson 2003) Equatorial Pacific, ΔpCO_2 is similar to or slightly lower than modern during the LGM, then shows a dramatic increase during the deglaciation, interpreted as an increase in the CO_2 content of upwelled waters. In the Indian Ocean, $\delta^{11}B$ records have been used to show variability in CO_2 outgassing related to different monsoon conditions (Naik et al. 2015; Palmer et al. 2010), with a peak in outgassing in the Bølling-Allerød interstadial, associated with an invigorated SW/Summer monsoon.

At high latitudes Yu et al. (2013) show that North Atlantic surface waters remained a sink of CO_2 from the atmosphere for the last 18 kyr. In contrast Southern Ocean surface waters saw pulses of high CO_2 during the last deglaciation (Martínez-Botí et al. 2015b), coincident with increases in atmospheric CO_2. This provides the first direct evidence for the role of the Southern Ocean in driving deglacial CO_2 rise, likely as a result of enhanced upwelling of CO_2-rich deep waters; the advection of these waters to the subsurface of the East Equatorial Pacific may also explain the pulses of CO_2 outgassing seen in this region (Martínez-Botí et al. 2015b; Fig. 5.10).

Boron isotope records from benthic foraminifera have also been used to examine the deep ocean carbonate system over the last deglaciation. These might be expected to show a pattern of increased deep ocean pH during intervals of CO_2 release from the deep ocean to the atmosphere. However Rae et al. (2014)'s data from the deep North Pacific show the opposite (Fig. 5.10d), with pulses of low pH during CO_2 rise in HS1 and the Younger Dryas. These are interpreted to result from mixing of CO_2-rich water from mid depths through the water column during pulses of local deep water formation (supported by comparison to radiocarbon and $\delta^{13}C$ data). This emphasizes the importance of considering changes in circulation, as well biogeochemistry, in interpreting benthic $\delta^{11}B$ records.

5.5.2 pH and CO_2 Beyond the Ice Cores

The reconstruction of atmospheric CO_2 change beyond the reach of the ice cores has been a major goal for studies using foraminiferal $\delta^{11}B$. Applications of such data include understanding the major climate transitions as Earth evolved from greenhouse to icehouse over the Cenozoic (Pearson et al. 2009; Bartoli et al. 2011; Fig. 5.6), to determining climate sensitivity in a warmer world (Anagnostou et al. 2016; Martínez-Botí et al. 2015a).

Early applications of foraminiferal $\delta^{11}B$ to reconstruct long term changes in surface ocean pH and atmospheric CO_2 indicated substantial decrease in CO_2 over the Cenozoic (Spivack et al. 1993; Pearson and Palmer 1999, 2000). However Pearson and Palmer (2000)'s iconic $\delta^{11}B$-CO_2 record also shows high amplitude spikes in the Palaeogene, and low and constant values in the Neogene (Fig. 5.6), leading to some suggestions that CO_2 and climate were decoupled (Shevenell et al. 2004; Pagani et al. 2005b; Mosbrugger et al. 2005).

More recent work shows high CO_2 values ($\sim$1500 ppm) during the early Eocene climatic optimum (EECO), which then decrease through the rest of the Eocene (Anagnostou et al. 2016). At higher resolution, Penman et al. (2014) use $\delta^{11}B$ to provide the first direct evidence of ocean acidification during the PETM, while Pearson

et al. (2009) show decreasing CO_2 levels over the Eocene-Oligocene boundary, though with an intriguing re-bound following Antarctic ice growth in the early Oligocene. In the Miocene, Foster et al. (2012) show a close coupling between atmospheric CO_2 and global climate and sea level (Fig. 5.8), which is also observed at higher temporal resolution (Fig. 5.6; Greenop et al. 2014; Badger et al. 2013).

A strong link between CO_2 and climate has also been shown using foraminiferal $\delta^{11}B$ in the Pliocene and early Pleistocene (Fig. 5.6). Seki et al. (2010), Bartoli et al. (2011) and Martínez-Botí et al. (2015a) show that the Pliocene warm period had CO_2 levels of ~400 ppm, similar to modern day anthropocene values. Martínez-Botí et al. (2015a) further quantify the relationship between CO_2 and climate at high resolution over this interval, and show that Earth System climate sensitivity in this warmer climate was half that of the Pleistocene. This can be attributed to a reduced ice-albedo feedback in the Pliocene, with equilibrium climate sensitivity found to be the same in both intervals when ice volume changes are considered. Between the Pliocene and the Pleistocene CO_2 falls (Seki et al. 2010; Bartoli et al. 2011), and Honisch et al. (2009) show that further intensification of glaciation during the mid-Pleistocene transition was linked to lower CO_2 in glacial periods, while CO_2 in interglacials remained relatively similar (Fig. 5.6).

5.6 Summary and Outlook

Recent developments in boron isotope analyses have spurred on an exciting era in the development and application of the boron isotope pH proxy in foraminifera. Boron isotope analysis by column chromatography and MC-ICPMS now gives reproducibility of ~0.2‰, equivalent to ~0.02 pH units, on around 5–20 benthic or 50–200 planktic foraminifera. Calibration studies show that foraminiferal $\delta^{11}B$ lies close to that of borate ion at seawater pH, consistent with simple models of $\delta^{11}B$-pH systematics based on sole incorporation of the borate ion into foraminiferal carbonate. Offsets between foraminifera and borate ion are largely attributable to modification of the local microenvironment by photosynthesis, respiration, and calcification. pH elevation during biomineralisation might be expected to drive substantial elevation of foraminiferal $\delta^{11}B$ above seawater borate, but this is not observed in the majority of species. The majority of the boron incorporated into foraminiferal calcite appears to be derived from borate ion at or close to seawater pH, providing an important constraint on models of biomineralisation.

Given the close coupling between seawater pH and CO_2, foraminiferal $\delta^{11}B$ measurements may provide relatively precise constraints on past CO_2 change, even with conservative estimates of a second carbonate system parameter. Boron isotope-based CO_2 reconstructions show a close match to the ice core CO_2 record where these overlap. On glacial-interglacial timescales, $\delta^{11}B$ records from regions of CO_2 disequilibrium in the surface ocean and in the deep ocean provide evidence of deglacial CO_2 release from the Southern Ocean and North Pacific, and changes in upwelled CO_2 in the tropics. Beyond the reach of the ice cores, foraminiferal $\delta^{11}B$ records increasingly demonstrate coupling between CO_2 and climate over key intervals of the last 60 Myr.

Future work should continue to refine boron isotope calibration in foraminifera, capitalize on boron's constraints on biomineralisation, and further constrain the evolution of seawater $\delta^{11}B$ to improve long-term pH and CO_2 reconstructions.

Acknowledgements This chapter was greatly improved thanks to detailed and thoughtful reviews by Marcus Gutjahr and an anonymous reviewer, editorial comments by Gavin Foster, and informal reviews by David Evans and Rosanna Greenop. Other members of the STAiG lab boron group, including Will Gray, Ben Taylor, Jessica Crumpton-Banks, Eloise Littley, and Matt Kaminski, along with the "B-team" at Southampton, are thanked for their hard work developing boron isotopes in foraminifera. Discussions over the last ten years with Michael Henehan, Gavin Foster, Richard Zeebe, Tim Elliott, Wally Broecker, Andy Ridgwell, Daniela Schmidt, Bärbel Hönisch, Kat Allen, Jess Adkins, and Jonathan Erez have all greatly contributed to my thinking about boron isotopes in foraminifera and CO_2 reconstruction; though any omissions or mistakes are mine alone. This work was partially supported by a research

fellowship from the University of St Andrews, $100 (pending) from Richard Zeebe, and NERC grants NE/N003861/1 and NE/N011716/1.

References

Al-Ammar AS, Gupta RK, Barnes RM (2000) Elimination of boron memory effect in inductively coupled plasma-mass spectrometry by ammonia gas injection into the spray chamber during analysis. Spectrochim Acta Part B 55(6):629–635

Allen KA et al (2011) Controls on boron incorporation in cultured tests of the planktic foraminifer Orbulina universa. Earth Planet Sci Lett 309(3–4):291–301

Allen KA et al (2016) Trace element proxies for surface ocean conditions: a synthesis of culture calibrations with planktic foraminifera. Geochem Cosmochim Acta 193:197–221

Allison N, Finch AA (2010) $\delta^{11}B$, Sr, Mg and B in a modern porites coral: the relationship between calcification site pH and skeletal chemistry. Geochim Cosmochim Acta 74(6):1790–1800

Allison N et al (2014) Corals concentrate dissolved inorganic carbon to facilitate calcification. Nat Commun 5:1–6.

Anagnostou E et al (2012) Evaluation of boron isotope ratio as a pH proxy in the deep sea coral Desmophyllum dianthus: evidence of physiological pH adjustment. Earth Planet Sci Lett 349–350:251–260

Anagnostou E et al (2016) Changing atmospheric CO_2 concentration was the primary driver of early Cenozoic climate. Nature 533(7603):380–384

Archer D, Maier-Reimer E (1994) Effect of deep-sea sedimentary calcite preservation on atmospheric CO_2 concentration. Nature 367:260–263

Badger MPS et al (2013) CO_2 drawdown following the middle Miocene expansion of the Antarctic ice sheet. Paleoceanography 28(1):42–53

Balan E et al (2016) First-principles study of boron speciation in calcite and aragonite. Geochem Cosmochim Acta 193:119–131

Barker S, Greaves M, Elderfield H (2003) A study of cleaning procedures used for foraminiferal Mg/Ca paleothermometry. Geochem Geophys Geosyst 4 (9):8407

Bartoli G, Hönisch B, Zeebe RE (2011) Atmospheric CO_2 decline during the Pliocene intensification of Northern Hemisphere glaciations. Paleoceanography 26(4):n/a

Bentov S, Erez J (2006) Impact of biomineralization processes on the Mg content of foraminiferal shells: a biological perspective. Geochem Geophys Geosyst 7 (1):1–11

Bentov S, Brownlee C, Erez J (2009) The role of seawater endocytosis in the biomineralization process in calcareous foraminifera. PNAS 106(51):21500–21504

Bereiter B et al (2015) Revision of the EPICA Dome C CO_2 record from 800 to 600 kyr before present. Geophys Res Lett 42(2):542–549

Bijma J, Faber WW, Hemleben C (1990) Temperature and salinity limits for growth and survival of some planktonic foraminifers in laboratory cultures. J. Foraminiferal Res 20(2):95–116

Bijma J, Hönisch B, Zeebe RE (2002) Impact of the ocean carbonate chemistry on living foraminiferal shell weight: comment on "Carbonate ion concentration in glacial-age deep waters of the Caribbean Sea" by W.S. Broecker and E. Clark. Geochem Geophys Geosyst 3 (11):1–7

Boyle EA (1981) Cadmium, zinc, copper, and barium in foraminifera tests. Earth Planet Sci Lett 53(1):11–35

Branson O et al (2015) The coordination and distribution of B in foraminiferal calcite. Earth Planet Sci Lett 416 (C):67–72

Broecker WS (2005) The role of the ocean in climate yesterday, today and tomorrow. Eldigio Press

Broecker WS, Peng TH (1987) The role of $CaCO_3$ compensation in the glacial to interglacial atmospheric CO_2 change. Global Biogeochem Cycles 1:15–29

Brumsack HJ, Zuleger E (1992) Boron and boron isotopes in pore waters from ODP Leg 127, Sea of Japan. Earth Planet Sci Lett 113(3):427–433

Corliss BH (1985) Microhabitats of benthic foraminifera within deep-sea sediments. Nature 314(6010):435–438

de Nooijer LJ, Langer G et al (2009a) Physiological controls on seawater uptake and calcification in the benthic foraminifer Ammonia tepida. Biogeosciences 6:2669–2675

de Nooijer LJ, Toyofuku T, Kitazato H (2009b) Foraminifera promote calcification by elevating their intracellular pH. Proc Nat Acad Sci 106(36):15374–15379

de Nooijer LJ et al (2014) Biomineralization in perforate foraminifera. Earth Sci Rev 135:48–58

Deyhle A, Kopf A (2004) Possible influence of clay contamination on B isotope geochemistry of carbonaceous samples. Appl Geochem 19(5):737–745

Dickson AG (1990) Thermodynamics of the dissociation of boric acid in synthetic seawater from 273.15 to 318.15 K. Deep Sea Res Part A Oceanogr Res Pap 37 (5):755–766

Dickson AG, Sabine CL, Christian JR (eds) (2007) Guide to best practices for ocean CO_2 measurements. PICES special publication 3. North Pacific Marine Science Organization, Sidney, p 176

Edgar KM et al (2015) Assessing the impact of diagenesis on d11B, $\delta^{13}C$, $\delta^{18}O$, Sr/Ca and B/Ca values in fossil planktic foraminiferal calcite. Geochim Cosmochim Acta 166(C):189–209

EPICA (2004) Eight glacial cycles from an Antarctic ice core. Nature 429(6992):623–628

Erez J (2003) The source of ions for biomineralization in foraminifera and their implications for paleoceanographic proxies. Rev Min Geochem 54(1):115–149

Farmer J et al (2015) Outside the pH box: boron isotopes in synthetic calcite precipitated under varying solution chemistry. In: AGU fall meeting abstracts. AGU

Farmer JR, Hönisch B, Uchikawa J (2016) Single laboratory comparison of MC-ICP-MS and N-TIMS boron isotope analyses in marine carbonates. Chem Geol 447:173–182

Feldmeijer W et al (2013) The effect of chemical pretreatment of sediment upon foraminiferal-based proxies. Geochem Geophys Geosyst 14(10): 3996–4014

Fietzke J et al (2010) Boron isotope ratio determination in carbonates via LA-MC-ICP-MS using soda-lime glass standards as reference material. J Anal At Spectrom 25 (12):1953–1957

Fietzke J et al (2015) Century-scale trends and seasonality in pH and temperature for shallow zones of the Bering Sea. Proc Natl Acad Sci 112(10):2960–2965

Foster GL (2008) Seawater pH, pCO_2 and $[CO_3=]$ variations in the Caribbean Sea over the last 130 kyr: a boron isotope and B/Ca study of planktic foraminifera. Earth Planet Sci Lett 271(1–4):254–266

Foster GL, Rae JWB (2016) Reconstructing ocean pH with boron isotopes in foraminifera. Ann Rev Earth Planet Sci 44(1):207–237. doi:10.1146/annurev-earth-060115-012226

Foster GL, Sexton PF (2014) Enhanced carbon dioxide outgassing from the eastern equatorial Atlantic during the last glacial. Geology 42(11):1003–1006

Foster GL, Pogge von Strandmann PAE, Rae JWB (2010) Boron and magnesium isotopic composition of seawater. Geochem Geophys Geosyst 11(8):Q08015

Foster GL, Lear CH, Rae JWB (2012) The evolution of pCO_2, ice volume and climate during the middle Miocene. Earth Planet Sci Lett 341–344:243–254

Foster GL et al (2013) Interlaboratory comparison of boron isotope analyses of boric acid, seawater and marine $CaCO_3$ by MC-ICPMS and NTIMS. Chem Geol 358:1–14

Gaillardet J, Lemarchand D, Göpel C (2001) Evaporation and sublimation of boric acid: application for boron purification from organic rich solutions. Geostand Geoanal Res 25(1):67–75

Gagnon AC, Adkins JF, Erez J, Eiler JM (2013) Sr/Ca sensitivity to aragonite saturation state in cultured subsamples from a single colony of coral: mechanism of biomineralization during ocean acidification. Geochem Cosmochim Acta 105:240–254

Glas MS, Fabricius KE et al (2012a) The O_2, pH and Ca^{2+} microenvironment of benthic foraminifera in a high CO_2 world. PLoS ONE 7(11):e50010

Glas MS, Langer G, Keul N (2012b) Calcification acidifies the microenvironment of a benthic foraminifer (*Ammonia* sp.). J Exp Mar Biol Ecol 424–425:53–58

Greenop R et al (2014) Middle Miocene climate instability associated with high-amplitude CO_2 variability. Paleoceanography 29(9):845–853

Greenop R et al (2017) A record of Neogene seawater $\delta^{11}B$ reconstructed from paired $\delta^{11}B$ analyses on benthic and planktic foraminifera. Clim Past 13:149–170

Gutjahr M et al (2014) Boron isotope intercomparison project (BIIP): development of a new carbonate standard for stable isotopic analyses. In: EGU general assembly conference abstracts, vol 16

Hain MP et al (2015) The effects of secular calcium and magnesium concentration changes on the thermodynamics of seawater acid/base chemistry: implications for eocene and cretaceous ocean carbon chemistry and buffering. Global Biogeochem Cycles 29(5):517–533

Hemleben C, Bijma J (1994) Foraminiferal population dynamics and stable carbon isotopes. In: Carbon cycling in the glacial ocean: constraints on the ocean's role in global change. Springer, Berlin, Heidelberg, pp 145–166

Hemleben C, Spindler M, Anderson OR (2012) Modern planktonic foraminifera. Springer Science & Business Media, New York, NY

Hemming NG, Hanson GN (1992) Boron isotopic composition and concentration in modern marine carbonates. Geochim Cosmochim Acta 56:537–543

Hemming NG, Hanson GN (1994) A procedure for the isotopic analysis of boron by negative thermal ionization mass spectrometry. Chem Geol 114(1–2):147–156

Hemming NG, Reeder RJ, Hanson GN (1995) Mineral-fluid partitioning and isotopic fractionation of boron in synthetic calcium carbonate. Geochim Cosmochim Acta 59(2):371–379

Henehan MJ et al (2013) Calibration of the boron isotope proxy in the planktonic foraminifera Globigerinoides ruber for use in palaeo-CO_2 reconstruction. Earth Planet Sci Lett 364:111–122

Henehan MJ et al (2016) A new boron isotope-pH calibration for Orbulina universa, with implications for understanding and accounting for "vital effects". Earth Planet. Sci. Lett. 454(C):282–292

Hershey JP et al (1986) The ionization of boric acid in NaCl, NaCaCl and NaMgCl solutions at 25 °C. Geochim Cosmochim Acta 50(1):143–148

Hönisch B, Hemming NG (2004) Ground-truthing the boron isotope-paleo-pH proxy in planktonic foraminifera shells: partial dissolution and shell size effects. Paleoceanography 19:PA4010

Hönisch B, Hemming NG (2005) Surface ocean pH response to variations in pCO_2 through two full glacial cycles. Earth Planet Sci Lett 236(1–2):305–314

Hönisch B et al (2003) The influence of symbiont photosynthesis on the boron isotopic composition of foraminifera shells. Mar Micropaleontol 49(1–2):87–96

Hönisch B et al (2004) Assessing scleractinian corals as recorders for paleo-pH: empirical calibration and vital effects. Geochim Cosmochim Acta 68(18):3675–3685

Hönisch B, Bickert T, Hemming NG (2008) Modern and Pleistocene boron isotope composition of the benthic foraminifer Cibicidoides wuellerstorfi. Earth Planet Sci Lett 272(1–2):309–318

Hönisch B et al (2009) Atmospheric carbon dioxide concentration across the mid-pleistocene transition. Science 324(5934):1551–1554

Hönisch B et al (2012) The geological record of ocean acidification. Science 335(6072):1058–1063

Horita J, Zimmermann H, Holland HD (2002) Chemical evolution of seawater during the Phanerozoic: implications from the record of marine evaporites. Geochim Cosmochim Acta 66(21):3733–3756

Jorgensen BB et al (1985) Symbiotic photosynthesis in a planktonic foraminifera, globigerinoides sacculifer (Brady), studied with microelectrodes. Limnol Oceanogr 30:1253–1267

Kaczmarek K et al (2015) Boron incorporation in the foraminifer Amphistegina lessonii under a decoupled carbonate chemistry. Biogeosciences 12:1753–1763

Kaczmarek K et al (2016) Investigating the effects of growth rate and temperature on the B/Ca ratio and $\delta^{11}B$ during inorganic calcite formation. Chem Geol 421(C):81–92

Kakihana H, Kotaka M (1977) Equilibrium constants for boron isotope-exchange reactions. Bull Res Lab Nucl React 2:1–12

Kasemann SA et al (2009) In situ boron isotope analysis in marine carbonates and its application for foraminifera and palaeo-pH. Chem Geol 260(1–2):138–147

Katz ME et al (2010) Traditional and emerging geochemical proxies in foraminifera. J Foramin Res 40(2):165–192

Kiss E (1988) Ion-exchange separation and spectrophotometric determination of boron in geological materials. Anal Chim Acta 211:243–256

Klochko K et al (2006) Experimental measurement of boron isotope fractionation in seawater. Earth Planet Sci Lett 248(1–2):276–285

Klochko K et al (2009) Re-evaluating boron speciation in biogenic calcite and aragonite using ^{11}B MAS NMR. Geochim Cosmochim Acta 73(7):1890–1900

Kohfeld KE, Ridgwell A (2009) Glacial-interglacial variability in atmospheric CO_2. In: Saltzman E, Quere CL (eds) Surface ocean-lower atmospheres processes. Geophysical monograph series. AGU, Washington DC

Köhler-Rink S, Kühl M (2000) Microsensor studies of photosynthesis and respiration in larger symbiotic foraminifera. I The physico-chemical microenvironment of Marginopora vertebralis, Amphistegina lobifera and Amphisorus hemprichii. Mar Biol 137 (3):473–486

Kotaka M, Kakihana H (1977) Thermodynamic isotope effect of trigonal planar and tetrahedral species. Bull Res Lab Nucl React 2:13–29

Krief S et al (2010) Physiological and isotopic responses of scleractinian corals to ocean acidification. Geochem Cosmochim Acta 74(17):4988–5001

Lear CH, Mawbey EM, Rosenthal Y (2010) Cenozoic benthic foraminiferal Mg/Ca and Li/Ca records: Toward unlocking temperatures and saturation states. Paleoceanography 25(4):PA4215

Lemarchand D et al (2000) The influence of rivers on marine boron isotopes and implications for reconstructing past ocean pH. Nature 408(6815):951–954

Lemarchand D et al (2002) An optimized procedure for boron separation and mass spectrometry analysis for river samples. Chem Geol 182(2–4):323–334

Liu Y, Tossell JA (2005) Ab initio molecular orbital calculations for boron isotope fractionations on boric acids and borates. Geochim Cosmochim Acta 69 (16):3995–4006

Lombard F et al (2010) Effect of carbonate ion concentration and irradiance on calcification in planktonic foraminifera. Biogeosciences 7:247–255

Lutze GF, Thiel H (1987) Cibicidoides wuellerstorfi and Planulina ariminensis, elevated epibenthic Foraminifera. In: Altenbach AV, Lutze GF, Weinholz, P (eds) Beobachtungen an Benthos-Foraminiferen (Teilprojekt A3). Berichte aus dem Sonderforschungsbereich 313 "Sedimentation im Europäischen Nordmeer". Sonderforschungsbereich 313, Universität Kiel, Keil, pp 17–30

Martínez-Botí MA, Foster GL et al (2015a) Plio-Pleistocene climate sensitivity evaluated using high-resolution CO_2 records. Nature 518(7537):49–54

Martínez-Botí MA, Marino G et al (2015b) Boron isotope evidence for oceanic carbon dioxide leakage during the last deglaciation. Nature 518(7538):219–222

Mavromatis V et al (2015) Characterization of boron incorporation and speciation in calcite and aragonite from co-precipitation experiments under controlled pH, temperature and precipitation rate. Geochim Cosmochim Acta 150:299–313

McCulloch M, Falter J et al (2012a) Coral resilience to ocean acidification and global warming through pH up-regulation. Nat Clim Change 2(8):623–627

McCulloch M, Trotter J et al (2012b) Resilience of cold-water scleractinian corals to ocean acidification: boron isotopic systematics of pH and saturation state up-regulation. Geochim Cosmochim Acta 87:21–34

Misra S et al (2014) Determination of $\delta^{11}B$ by HR-ICP-MS from mass limited samples: application to natural carbonates and water samples. Geochem Cosmochim Acta 140:531–552

Morard R et al (2009) Morphological recognition of cryptic species in the planktonic foraminifer Orbulina universa. Mar Micropaleontol 71(3–4):148–165

Mosbrugger V, Utescher T, Dilcher DL (2005) Cenozoic continental climatic evolution of Central Europe. Proc Natl Acad Sci U S A 102(42):14964–14969.

Naik SS et al (2015) Tracing the strength of the southwest monsoon using boron isotopes in the eastern Arabian Sea. Geophys Res Lett 42(5):1450–1458

Nehrke G et al (2013) A new model for biomineralization and trace-element signatures of Foraminifera tests. Biogeosciences 10(10):6759–6767

Ni Y et al (2007) A core top assessment of proxies for the ocean carbonate system in surface dwelling foraminifers. Paleoceanography 22(3):PA3212

Ni Y, Foster GL, Elliott T (2010) The accuracy of $\delta^{11}B$ measurements of foraminifers. Chem Geol 274(3–4):187–195

Nir O et al (2015) Direct measurement of the boron isotope fractionation factor: reducing the uncertainty in reconstructing ocean paleo-pH. Earth Planet Sci Lett 414(C):1–5

Noireaux J et al (2015) Crystallographic control on the boron isotope paleo-pH proxy. Earth Planet Sci Lett 430(C):398–407

Oi T (2000) Calculations of reduced partition function ratios of monomeric and dimeric boric acids and borates by the ab initio molecular orbital theory. J Nucl Sci Technol 37(2):166–172

Pagani M, Lemarchand D et al (2005a) A critical evaluation of the boron isotope-pH proxy: The accuracy of ancient ocean pH estimates. Geochim Cosmochim Acta 69(4):953–961

Pagani M, Zachos JC et al (2005b) Marked decline in atmospheric carbon dioxide concentrations during the paleogene. Science 309(5734):600–603

Palmer MR, Pearson PN (2003) A 23,000-year record of surface water pH and pCO_2 in the western equatorial Pacific Ocean. Science 300(5618):480–482

Palmer MR, Pearson PN, Cobb SJ (1998) Reconstructing past ocean pH-depth profiles. Science 282(5393):1468

Palmer MR et al (2010) Multi-proxy reconstruction of surface water pCO_2 in the northern Arabian Sea since 29ka. Earth Planet Sci Lett 295(1–2):49–57

Paris G, Bartolini A et al (2010a) Investigating boron isotopes in a middle Jurassic micritic sequence: primary vs. diagenetic signal. Chem Geol 275(3–4):117–126

Paris G, Gaillardet J, Louvat P (2010b) Geological evolution of seawater boron isotopic composition recorded in evaporites. Geology 38(11):1035–1038

Pearson P, Palmer MR (1999) Middle Eocene seawater pH and atmospheric carbon dioxide concentrations. Science 284:1824–1826

Pearson PN, Palmer MR (2000) Atmospheric carbon dioxide concentrations over the past 60 million years. Nature 406:695–699

Pearson PN, Foster GL, Wade BS (2009) Atmospheric carbon dioxide through the Eocene-Oligocene climate transition. Nature 461(7267):1110–1113

Penman DE et al (2014) Rapid and sustained surface ocean acidification during the Paleocene-Eocene thermal maximum. Paleoceanography 29(5):357–369

Rae JWB et al (2011) Boron isotopes and B/Ca in benthic foraminifera: proxies for the deep ocean carbonate system. Earth Planet Sci Lett 302(3–4):403–413

Rae JWB et al (2014) Deep water formation in the North Pacific and deglacial CO_2 rise. Paleoceanography 29 (6):645–667

Raitzsch M, Hönisch B (2013) Cenozoic boron isotope variations in benthic foraminifers. Geology 41(5):591–594

Raitzsch M et al (2010) Incorporation of Mg and Sr in calcite of cultured benthic foraminifera: impact of calcium concentration and associated calcite saturation state. Biogeosciences 7(3):869–881

Raitzsch M et al (2011) Modern and late Pleistocene B/Ca ratios of the benthic foraminifer Planulina wuellerstorfi determined with laser ablation ICP-MS. Geology 39(11):1039–1042

Ridgwell A (2005) A mid mesozoic revolution in the regulation of ocean chemistry. Mar Geol 217(3–4):339–357

Rink S et al (1998) Microsensor studies of photosynthesis and respiration in the symbiotic foraminifer Orbulina universa. Mar Biol 131(4):583–595

Rollion-Bard C, Erez J (2010) Intra-shell boron isotope ratios in the symbiont-bearing benthic foraminiferan Amphistegina lobifera: Implications for $\delta^{11}B$ vital effects and paleo-pH reconstructions. Geochim Cosmochim Acta 74(5):1530–1536

Rollion-Bard C et al (2011) Boron isotopes as pH proxy: a new look at boron speciation in deep-sea corals using ^{11}B MAS NMR and EELS. Geochim Cosmochim Acta 75(4):1003–1012

Rosner M, Romer RL, Meixner A (2005) Air handling in clean laboratory environments: the reason for anomalously high boron background levels. Anal Bioanal Chem 382(1):120–124

Russell AD et al (2004) Effects of seawater carbonate ion concentration and temperature on shell U, Mg, and Sr in cultured planktonic foraminifera. Geochim Cosmochim Acta 68(21):4347–4361

Rustad JR, Bylaska EJ (2007) Ab initio calculation of isotopic fractionation in B(OH)3(aq) and $B(OH)_4^-$(aq). J Am Chem Soc 129(8):2222–2223

Sadekov A et al (2016) Understanding the mechanisms behind boron elemental and isotopic fractionation in the benthic foraminifera Cibicidoides wuellerstorfi. In: ICP12. Utrecht

Sanyal A, Bijma J (1999) A comparative study of northwest Africa and eastern equatorial Pacific upwelling zones as sources of CO_2 during glacial periods based on boron isotope paleo-pH estimation. Paleoceanography 14(6):753–759

Sanyal A et al (1995) Evidence for a higher pH in the glacial ocean from boron isotopes in foraminifera. Nature 373:234–236

Sanyal A et al (1996) Oceanic pH control on the boron isotopic composition of foraminifera: evidence from culture experiments. Paleoceanography 11(5):513–517

Sanyal A et al (1997) Changes in pH in the eastern equatorial Pacific across stage 5–6 boundary based on boron isotopes in foraminifera. Global Biogeochem Cycles 11:125–133

Sanyal A et al (2001) Empirical relationship between pH and the boron isotopic composition of Globigerinoides sacculifer: implications for the boron isotope paleo-pH proxy. Paleoceanography 16(5):515–519

Sarmiento JL, Gruber N (2006) Ocean biogeochemical dynamics. Cambridge University Press

Schmidt MW, Spero HJ, Lea DW (2004) Links between salinity variation in the Caribbean and North Atlantic thermohaline circulation. Nature 428:160–163

Schmidt MW, Vautravers MJ, Spero HJ (2006) Western Caribbean sea surface temperatures during the late quaternary. Geochem Geophys Geosyst 7:Q02P10. doi:10.1029/2005GC000957

Seki O et al (2010) Alkenone and boron-based Pliocene pCO_2 records. Earth Planet Sci Lett 292(1–2):201–211

Sen S et al (1994) Coordination environments of B-impurities in calcite and aragonite polymorphs—a B-11 Mas Nmr-study. Am Miner 79(9–10):819–825

Shevenell AE, Kennett JP, Lea DW (2004) Middle Miocene Southern ocean cooling and Antarctic cryosphere expansion. Science 304:1766–1770

Sigman DM, McCorkle DC, Martin WR (1998) The calcite lysocline as a constraint on glacial/interglacial low-latitude production changes. Global Biogeochem Cycles 12(3):409–427

Sigman DM, Hain MP, Haug GH (2010) The polar ocean and glacial cycles in atmospheric CO_2 concentration. Nature 466(7302):47–55

Simon L et al (2006) Modelling the geochemical cycle of boron: implications for the long-term $\delta^{11}B$ evolution of seawater and oceanic crust. Chem Geol 225(1–2):61–76

Smith HJ et al (1995) The boron isotopic composition of altered oceanic crust. Chem Geol 126(2):119–135

Spero HJ et al (2015) Timing and mechanism for intratest Mg/Ca variability in a living planktic foraminifer. Earth Planet Sci Lett 409:32–42

Spezzaferri S et al (2015) Fossil and genetic evidence for the polyphyletic nature of the planktonic foraminifera "globigerinoides," and description of the new genus Trilobatus. In: Abramovich S (ed) PLOS One 10(5): e0128108

Spivack AJ, Edmond JM (1987) Boron isotope exchange between seawater and the oceanic crust. Geochim Cosmochim Acta 51(5):1033–1043

Spivack AJ, Palmer MR, Edmond JM (1987) The sedimentary cycle of the boron isotopes. Geochim Cosmochim Acta 51(7):1939–1949

Spivack AJ, You CF, Smith HJ (1993) Foraminiferal boron isotope ratios as a proxy for surface ocean pH over the past 21 Myr. Nature 363:149–151

Stewart JA, Anagnostou E, Foster GL (2016) An improved boron isotope pH proxy calibration for the deep-sea coral Desmophyllum dianthus through sub-sampling of fibrous aragonite. Chem Geol 447:148–160

Su C, Suarez DL (1995) Coordination of adsorbed boron: a FTIR spectroscopic study. Environ Sci Technol 29(2):302–311

Toyofuku T et al (2008) Real-time visualization of calcium ion activity in shallow benthic foraminiferal cells using the fluorescent indicator Fluo-3 AM. Geochem Geophys Geosyst 9(5):Q05005

Toyofuku T et al (2017) Proton pumping accompanies calcification in foraminifera. Nat Commun 8:1–6

Trotter J, Montagna P, McCulloch M, Silenzi S, Reynaud S, Mortimer G et al (2011) Quantifying the pH 'vital effect' in the temperate zooxanthellate coral Cladocora caespitosa: validation of the boron seawater pH proxy. Earth Planet Sci Lett 303:163–173

Tyrrell T, Zeebe RE (2004) History of carbonate ion concentration over the last 100 million years. Geochim Cosmochim Acta 68(17):3521–3530

Uchikawa J et al (2015) Experimental evidence for kinetic effects on B/Ca in synthetic calcite: Implications for potential $B(OH)_4^-$ and $B(OH)_3$ incorporation. Geochim Cosmochim Acta 150:171–191

van Heuven S et al (2009) MATLAB program developed for CO_2 system calculations. Carbon Dioxide Information Analysis Center, Oak Ridge National Laboratory, U.S. Department of Energy, Oak Ridge, Tennessee. doi:10.3334/CDIAC/otg.CO2SYS_MATLAB_v1.1

Venn A et al (2011) Live tissue imaging shows reef corals elevate pH under their calcifying tissue relative to seawater. In: Vollmer S (ed) PLOS One 6(5):e20013

Vengosh A et al (1991) Coprecipitation and isotopic fractionation of boron in modern biogenic carbonates. Geochim Cosmochim Acta 55(10):2901–2910

Vengosh A et al (1992) Boron isotope variations during fractional evaporation of sea water: new constraints on the marine vs. nonmarine debate. Geology 20(9):799–802

Wang B-S et al (2010) Direct separation of boron from Na- and Ca-rich matrices by sublimation for stable isotope measurement by MC-ICP-MS. Talanta 82(4):1378–1384

Wefer G et al (1999) Clues to ocean history: a brief overview of proxies. In: Fischer G, Wefer G (eds) Use of proxies in paleoceanography. Springer, Berlin, Heidelberg, New York, pp 1–68

Wei H-Z et al (2014) An improved procedure for separation/purification of boron from complex matrices and high-precision measurement of boron isotopes by positive thermal ionization and multicollector inductively coupled plasma mass spectrometry. Talanta 123:151–160

Wolf-Gladrow DA, Bijma J, Zeebe RE (1999) Model simulation of the carbonate chemistry in the microenvironment of symbiont bearing foraminifera. Mar Chem 64(3):181–198

Yoshimura K et al (1998) Complexation of boric acid with the N-methyl-D-glucamine group in solution and in crosslinked polymer. J Chem Soc Faraday Trans 94 (5):683–689

You C-F et al (1993) Mobilization of boron in convergent margins: implications for the boron geochemical cycle. Geology 21(3):207–210

Yu J, Elderfield H (2007) Benthic foraminiferal B/Ca ratios reflect deep water carbonate saturation state. Earth Planet Sci Lett 258(1–2):73–86

Yu J et al (2007) Preferential dissolution of benthic foraminiferal calcite during laboratory reductive cleaning. Geochem Geophys Geosyst 8(6):Q06016

Yu J et al (2010) An evaluation of benthic foraminiferal B/Ca and $\delta^{11}B$ for deep ocean carbonate ion and pH reconstructions. Earth Planet Sci Lett 293(1–2): 114–120

Yu J et al (2013) Calibration and application of B/Ca, Cd/Ca, and $\delta^{11}B$ in Neogloboquadrina pachyderma

(sinistral) to constrain CO_2 uptake in the subpolar North Atlantic during the last deglaciation. Paleoceanography 28:237–252
Zachos JC et al (2001) Trends, rhythms, and aberrations in global climate 65 Ma to present. Science 292:686–693
Zachos JC, Dickens GR, Zeebe RE (2008) An early Cenozoic perspective on greenhouse warming and carbon-cycle dynamics. Nature 451(7176):279–283
Zeebe RE (2005) Stable boron isotope fractionation between dissolved $B(OH)_3$ and $B(OH)_4$. Geochim Cosmochim Acta 69(11):2753–2766
Zeebe RE, Sanyal A (2002) Comparison of two potential strategies of planktonic foraminifera for house building: Mg^{2+} or H^+ removal? Geochim Cosmochim Acta 66(7):1159–1169
Zeebe RE, Wolf-Gladow DA (2001) CO_2 in seawater: equilibrium, kinetic, isotopes. Elsevier, Amsterdam
Zeebe RE et al (2001) A theoretical study of the kinetics of the boric acid-borate equilibrium in seawater. Mar Chem 73(2):113–124
Zeebe RE et al (2003) Vital effects in foraminifera do not compromise the use of $\delta^{11}B$ as a paleo-pH indicator: evidence from modeling. Paleoceanography 18(2):1043